Mémoire

Auteur : Devos, Valentine
Promoteur(s) : Dupret, Marc-Antoine
Faculté : Faculté des Sciences
Diplôme : Master en sciences spatiales, à finalité approfondie
Année académique : 2022-2023
URI/URL : http://hdl.handle.net/2268.2/18810

UNIVERSITY OF LIÈGE - FACULTY OF SCIENCES

TIDAL DEFORMATIONS IN BINARY STAR SYSTEMS

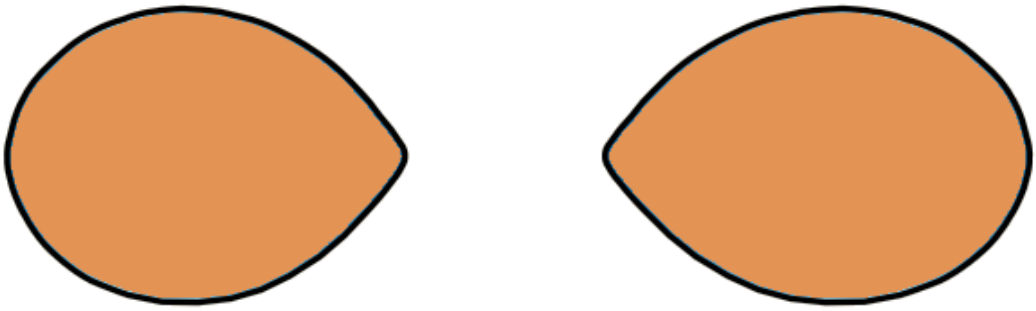

To obtain the master's degree in "Space Sciences",
by Valentine DEVOS.

Academic advisor: Marc-Antoine DUPRET.

ACADEMIC YEAR 2022-2023

Abstract

This work focused on the study of tidal deformations in binary star systems. More specifically, the first step is the complete development of the perturbative method, usually used to model this kind of system, in order to highlight the approximation made for the calculations. The second step is a comparison between this method and MoBiDICT, a new non-perturbative 3D static model that computes the deformation in binaries. Finally, those results will then be compared to a system already observed to assess them. The results show that the perturbative method underestimates the total potential of the system where the stars are highly distorted, and then underestimates different resulting parameters, such as the apsidal motion rate. Comparing with observational data, MoBiDICT gives close results concerning the apsidal motion rate. Finally, the influence of the α_{ov} parameter shows that the modification of the internal structure of the stars will directly influence the apsidal motion.

Keywords: binary star system, tidal interaction, perturbative method, MoBiDICT

Résumé

Ce travail s'est concentré sur l'étude des déformations de marée dans les systèmes d'étoiles binaires. Plus spécifiquement, la première étape consiste en le développement complet de la méthode perturbative, généralement utilisée pour modéliser ce type de système, afin de mettre en évidence les approximations effectuées pour les calculs. La deuxième étape consiste en une comparaison entre cette méthode et MoBiDICT, un nouveau modèle statique 3D non perturbatif qui calcule la déformation dans les systèmes binaires. Enfin, ces résultats seront ensuite comparés à un système déjà observé pour les évaluer. Les résultats montrent que la méthode perturbative sous-estime le potentiel total du système lorsque les étoiles sont fortement déformées, et sous-estime ensuite différents paramètres résultants, tels que le taux de mouvement des apsides. En comparant avec les données observationnelles, MoBiDICT donne des résultats proches en ce qui concerne le taux de mouvement des apsides. Enfin, l'influence du paramètre α_{ov} montre que la modification de la structure interne des étoiles influencera directement le mouvement des apsides.

Mots-clés : système d'étoiles binaires, interaction de marée, méthode perturbative, MoBiDICT

Acknowledgement

I want to express my gratitude to all those who have supported me throughout my journey in completing this master's thesis. First and foremost, I want to offer my sincere thanks to my thesis supervisor, Prof. Dr Marc-Antoine Dupret, whose guidance, expertise, and availability were instrumental in shaping the direction and quality of this work.

I want also to express my sincere gratitude to Loïc Fellay for his valuable discussions, guidance, and availability, which contributed significantly to the refinement of my ideas and methodologies.

I would also like to thank the members of my thesis committee for the time they will take to read this work, namely: Prof. Dr Gregor Rauw, Prof. Dr Jean-Marie Beckers, and Prof. Dr Valérie Van Grootel.

I offer sincere thanks to all my dear family, Francis, Stéphanie, Camille, and Gabriel, as well as my friends, Nicolas and Thomas, for their willingness to endure me through my whole education and life and for their unshakable faith in me. I also express my sincere thanks to my companion, Lucas, who always knew how to find the right words, support me and help me during all these years.

Lastly, I extend my appreciation to all the resources, libraries, and institutions that provided access to valuable research materials and data, enabling me to conduct a comprehensive study.

This work would not have been possible without the collective contributions and support of all these individuals, and for that, I am truly grateful.

Contents

List of Figures

List of Tables

Nomenclature

$\bar{\rho}$	Mean value of the density
χ	Centrifugal potential
$\dot{\omega}$	Apsidal motion rate
ϵ	Ellipticity
η	Structural coefficient
$\mathscr{R}$	Perturbed acceleration producing the apsidal motion
$\mathscr{R}_{\mathrm{c}}$	Perturbed acceleration from the centrifugal deformations
$\mathscr{R}_{\mathrm{tides}}$	Perturbed acceleration from the tidal deformations
μ	Reduced mass
Ω_0	Rotational speed of the star around the center of mass
Ω_{Ri}	Rotational speed of a star's element around the center the star
Φ_i	Gravitational potential due to the i^{th} star
ρ	Mass density
A	Semi-major axis of the elliptical orbit
a	Mean radius of the spheroid
a_i	Distance between the center of mass and the center of the i^{th} star
c	Light speed
CM	Center of Mass

e	Eccentricity
F_{ij}	Force acting by i^{th} star on j^{th}
G	Gravitational constant
$k_{l,i}$	Apsidal motion's constant
l, m	Respectively degree and order of the associated Legendre polynomial (integers)
M	Total mass
M_i	Mass of the i^{th} star
P	Star's element at which we observe some parameters
p	Fluid pressure
P_0	Rotational period of the eccentric orbit
$P_i(x)$	i^{th} Legendre Polynomial of parameter x
P_i	Rotational period of the i^{th} star
q	Mass ratio
r, θ, ϕ	Spherical coordinate system
R	Mean radius of the spheroid
R_e	Radius of the spheroid at the equator
r_i	Distance between the observation point and the center of the i^{th} star
R_p	Radius of the spheroid at the poles
s	Distance between one element and the center of its star
t	Time
U	Total potential
x, y, z	Cartesian coordinate system
$X_k^{n,m}$	Hansen coefficient
Y_l^m	Associated Legendre Polynomial

1 Introduction

Tidal deformation in binary star systems is a fascinating area of study that involves the analysis of how the gravitational forces between two stars can cause them to become distorted. As the stars orbit around each other, they experience tidal forces that can stretch or compress their shapes, leading to observable changes in their brightness and spectral properties.
This phenomenon is particularly relevant for close binary systems, where the stars are so close to each other that they can exchange material and affect each other's evolution. Tidal deformation can cause the stars to lose angular momentum, which can lead to their orbits decaying and eventually merging.
The study of tidal deformation in binary systems can provide important insights into stellar astrophysics, as it allows astronomers to better understand the physical processes that govern the behaviour of stars. It has also practical applications for the study of exoplanets, as the same tidal forces that affect binary stars can also influence the orbits and evolution of planets around other stars.
Researchers use a variety of observational and theoretical tools to study tidal deformation in binary star systems. This work developed in detail the perturbative method used to usually model binary systems. Then, a new non-perturbative method to compute the deformation of binaries in three dimensions, MoBiDICT, will be introduced. Finally, a comparison between observational data and MoBiDICT's results will be done to assess this new method.

In this introduction section, a general definition of binary star systems will be given. The classification, formation, and evolution of this kind of system will be explained, as well as the case of multiple-star systems and the possibility of the presence of planets. The objectives and outlines of the work will then be given. Finally, a literature review of previous work about tidal deformation and apsidal motion in binary star systems will be done.

1.1 Binary systems of stars

1.1.1 Definition

A system of binary stars is a celestial system consisting of two stars that are gravitationally bound to each other. These stars orbit a common center of mass, forming a binary system, as presented in Figure 1.1, where the primary star, i.e., the brightest component of the system, is presented in purple, and the secondary star, or the companion, is in blue. In this binary star system, the two stars can have a range of characteristics, including similar or different masses, sizes, and spectral types. They may be at various stages in their evolution, from protostars to main-sequence stars, giants, or even compact objects like white dwarfs, neutron stars, or black holes.

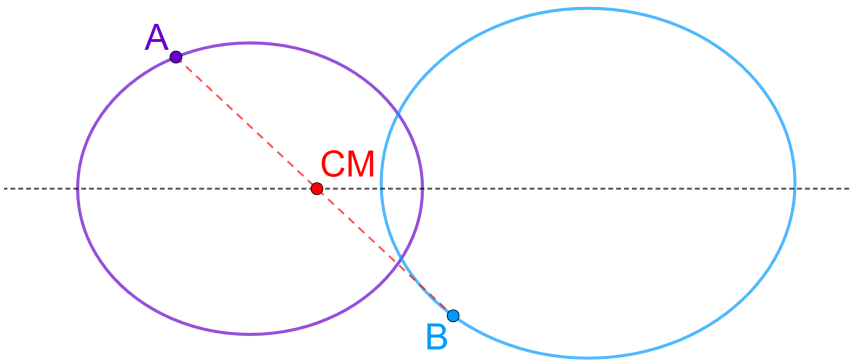

Figure 1.1: Schematic representation of a binary system of stars. In purple is presented the orbit of the primary star A, in blue the one of the secondary star B, and the CM in red is the center of mass of the system.

The stars in a binary system are held together by their mutual gravitational attraction, which determines their orbital motion. The orbit can have different shapes, ranging from nearly circular to highly elliptical. The orbital parameters, such as the period, eccentricity and inclination define the characteristics of the binary system. The gravitational interaction between the stars can affect their individual evolution, leading to phenomena such as mass

transfer, tidal deformation, stellar mergers, or the formation of compact binaries.

Binary star systems are prevalent in the universe, and they come in various types, including detached binaries, where stars are well-separated, semi-detached binaries, with mass transfer, and contact binaries, where the stars share a common envelope. The classification of binary systems is based on factors such as the separation between stars, the degree of interaction, and observational characteristics.

1.1.2 Classification

As already said, binary star systems can be classified based on various factors, mainly the separation between the stars, the degree of interaction, or the way they have been observed.

Separation-based Classification : This classification is based on the distance between both stars. One has:

- ⋆ Close Binaries: These systems have relatively small separations between the stars, typically a few astronomical units (AU) to a fraction of an AU. The stars are in close proximity and can interact strongly, often leading to phenomena like mass transfer or tidal effects.
- ⋆ Wide Binaries: In these systems, the stars are relatively far apart, typically separated by several tens or hundreds of AU. The gravitational interaction between the stars is relatively weak, and they typically evolve independently.

Interaction-based Classification : This classification is based on the type of interaction between the envelopes of both stars. In Figure 1.2 are illustrated the different configurations that are explained just below.

- ⋆ Detached Binaries: The stars in these systems have separate, non-overlapping Roche lobes and do not transfer mass between them. They have distinct shapes and do not share a common envelope.
- ⋆ Semidetached Binaries: In semidetached systems, one star fills its Roche lobe while the other does not. Mass transfer occurs from the overflowing star to its companion, leading to accretion and potentially affecting the evolution of both stars.
- ⋆ Contact Binaries: Contact binaries have stars that are so close that they share a common envelope. The stars distort their shapes, and they may exchange mass.

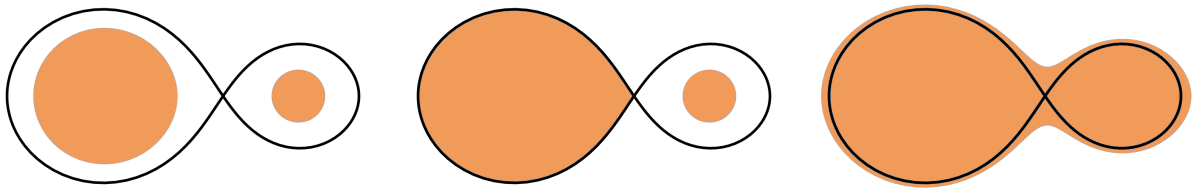

(a) Detached binaries (b) Semidetached binaries (c) Contact binaries

Figure 1.2: Illustration of the different interactions between stars in a binary system.

Observational Classification : This classification is generally the most used to classify binary stars as it considers their method of detection.

⋆ Visual Binaries: These binary systems can be directly resolved through telescopes, and the two stars can be seen as separate entities, as presented in Figure 1.3[1]. These systems are characterized by the ability to visually distinguish the two stars and measure their positions and motions independently. By tracking their motions, it is possible to derive their orbital parameters such as their periods, eccentricities and inclinations.

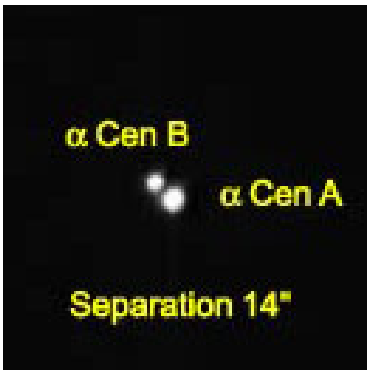

Figure 1.3: CCD image of the visual binary α Cen A and B. Credit: CSU Remote Telescope.

⋆ Spectroscopic Binaries: Spectroscopic techniques are used to study these systems, as they are too distant to be resolved separately by telescope. Spectroscopic binaries are identified by observing variations in the spectral lines of the combined light, which indicate the presence of two or more stars in orbit around each other. In a spectroscopic binary system, the motion of the stars along the line of sight causes a Doppler shift in their spectral lines. As the stars move toward or away from us during their orbital motion, the wavelengths of the spectral lines are shifted to shorter (blueshift) or longer (redshift) wavelengths, respectively. By measuring these Doppler shifts in the spectral lines, one can determine the radial velocity variations of the stars. The radial velocity curve, which shows how

[1] From http://www.csu.edu.au/telescope/ (10/07/23)

the radial velocity of the system changes over time, provides valuable information about the orbital parameters of the binary system, including the period, eccentricity, and mass ratio of the stars.

- ⋆ Eclipsing Binaries: Eclipsing binaries are systems where the stars orbit in such a way that they periodically eclipse each other from our line of sight. During an eclipse, one star passes in front of the other, partially or completely blocking its light. This results in a decrease in the total brightness of the system. By observing the variations in the system's light curve, one can derive valuable information about the properties of the stars and their orbital parameters. The time between consecutive eclipses corresponds to the orbital period of the system. The duration and depth of the eclipses provide insights into the relative sizes and shapes of the stars and their proximity to each other. If the eclipses have different durations or depths, it suggests that the orbit is not perfectly circular, indicating an eccentric orbit. Finally, by analyzing the shape and duration of the eclipses, one can determine the mass ratio of the stars, i.e. the ratio of the mass of the secondary star to the mass of the primary star.
- ⋆ Astrometric binaries: By monitoring certain stars over a period of time, we may notice a discernible deviation or "wobble" in their proper motion. When this deviation occurs periodically, it suggests that an invisible companion exerts a gravitational influence on the star. In such cases, we identify the presence of a binary system, wherein a visible star and a fainter companion orbit a shared center of mass. These binary systems, discovered through astrometric methods, are referred to as astrometric binaries. One can see in Figure 1.4[2] the proper motion of Sirius system over 80 years. F. Bessell shows in 1844 a wobble in its proper motion, suggesting the presence of a non-visible companion.

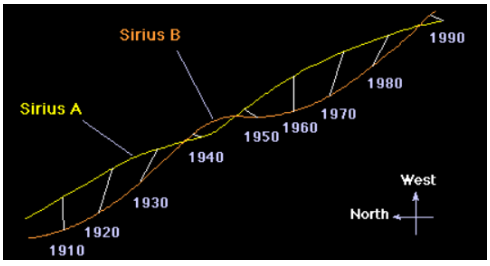

Figure 1.4: Diagram of the proper motion of the Sirius system over 80 years. The slight perturbations or wobble in the bright star, Sirius A, is due to the presence of its much dimmer white dwarf companion, Sirius B. Credit: Courtesy of Mike Guidry, University of Tennessee.

These classifications provide a framework for organizing and studying binary star systems. It is worth noting that some systems can fall into multiple categories, as their properties and behaviours may change over time.

[2] From https://www.atnf.csiro.au/outreach/education/senior/astrophysics/binary_types.html (10/07/23)

1.1.3 Formation

Binary star systems can be formed through various mechanisms, depending on the specific circumstances of their formation.

Fragmentation of a Molecular Cloud

Molecular clouds are vast regions of interstellar gas and dust with high densities and low temperatures. These clouds can undergo gravitational collapse, initiating the process of star formation. As the cloud contracts under its self-gravity, it can fragment into smaller clumps, each of which has the potential to collapse further and form individual stars.

During the fragmentation process, if the molecular cloud breaks into two or more clumps of similar mass, these clumps can collapse and form binary, or multiple, star systems. As proposed by J.E. Pringle [1], an external impulse will initiate the collapsing, and produce wide binaries.

S. Offner & al. [2] [3] suggest that turbulence within a single core leads to the formation of multiple dense clumps. Each clump then collapses independently, resulting in the formation of stars that orbit each other. Their team conducted a series of simulations using this kind of turbulent fragmentation to investigate the formation of binary star systems. They ran a total of twelve simulations, of which five produced single stars, five produced binaries, and two produced triple-star systems. These simulations started with a spherical core exhibiting random turbulent velocities and followed the process of seed formation, mass accretion, and protostellar outflow launching. Their results are consistent with the expectation of wide separations resulting from separate gravitational collapse events.

Disk Fragmentation

It is a process by which a protostellar disk surrounding a young star becomes gravitationally unstable and fragments into multiple clumps that can eventually form binary star systems. As explained by Kratter and Lodato [4], the disk fragmentation occurs when a protostellar disk becomes sufficiently massive and cool to reach a threshold for gravitational instability. This instability leads to the formation of dense clumps within the disk. These clumps can further contract and undergo gravitational collapse, potentially forming binary systems or multiple-star systems. Several factors influence the conditions under which disk fragmentation can occur, including the mass of the protostellar disk, its temperature, viscosity, and the presence of turbulence or magnetic fields. Disk fragmentation can occur through different fragmentation modes, such as gravitational fragmentation, gravitational instability in spiral arms, or disk fragmen-

tation due to disk warping or tidal forces from companion stars. Each mode has its specific conditions and outcomes.

Capture or Exchange

Binary systems can also form through capture or exchange interactions. The capture or exchange process for the formation of binary star systems occurs when a passing star interacts gravitationally with either a single star or an existing binary system, resulting in the capture of the passing star and the formation of a binary configuration. In the capture scenario, a single star encounters another star or a binary system closely enough that their gravitational interaction leads to the capture of the passing star into a binary system. The passing star's trajectory is altered, and it becomes gravitationally bound to the original star or binary, forming a new binary system. In the exchange scenario, the gravitational interaction between a binary system and a passing star can lead to the exchange of companions. During the interaction, one star from the binary is ejected, while the passing star becomes gravitationally bound to the remaining star in the binary, resulting in a new binary configuration. The likelihood of capture or exchange events depends on the stellar densities and velocities in stellar environments such as stellar clusters. The higher the density and velocity dispersion, the more opportunities for encounters and gravitational interactions that can result in capture or exchange events.

Stellar Collision

Binary star systems can sometimes form through stellar collisions, particularly in dense stellar environments such as stellar clusters. Stellar collisions occur when two stars physically collide with each other due to close encounters or interactions in dense stellar regions. These collisions can result in the merger of the two stars, leading to the formation of a more massive star or a binary star system. In dense stellar clusters, the proximity of stars increases the likelihood of close encounters and, consequently, stellar collisions. In the cores of such clusters, where stellar densities are highest, stellar collisions can occur more frequently, potentially resulting in the formation of binary systems. The outcome of a stellar collision depends on the masses, velocities, and impact parameters of the colliding stars. In some cases, the collision can lead to the coalescence of the stellar cores, forming a single, more massive star. In other cases, the collision can result in the formation of a binary star system, where the two stars remain gravitationally bound after the collision.

Those processes of formation are generally considered for low-mass binary systems. However, for massive binaries, the fragmentation of molecular cloud as well as the disk fragmentation can be thought about at the condition that one has a massive molecular cloud or protostellar disk. A competitive accretion scenario can also occur when multiple protostars

within a clustered environment compete for the available gas and dust in their vicinity. The most massive protostars can accrete material at a higher rate, which gives them a competitive advantage over their companions. Finally, in dense stellar environments, such as stellar clusters, close encounters and stellar collisions can occur. In some cases, collisions between massive stars can result in the coalescence of their cores, leading to the formation of a massive binary or hierarchical multiple system.

The case of close binaries is also particular, as it involves the close proximity of the two stars. The disk fragmentation process can lead to such a system, but other scenarios can also be considered. The obvious situation is the capture by the gravitational interaction of a passing star with another. A stellar collision can also be considered for the formation of close binaries. Tidal interactions can cause two stars to migrate closer to each other, by the gravitational influence of a third passing star. Finally, close binaries can also form through dynamical interactions in stellar clusters. Interactions between stars can exchange companions, leading to the formation of new binary systems with close separations. Additionally, gravitational interactions can cause orbital decay, bringing initially wider binary systems into close configurations.

While the exact mechanisms responsible for the formation of binaries are still being investigated, it is likely that a combination of these processes, as well as other factors such as environmental conditions and dynamical interactions, play a role in the formation and evolution of binary star systems.

1.1.4 Evolution

The evolution of a binary star system is influenced by several factors, including the masses of the stars, their separation, their orbital eccentricity, and the presence of other nearby objects. The stellar evolution of both stars is affected by the presence of their companion, especially by the interactions between them.

Interactions between stars in binary systems can have significant consequences for their stellar evolution. Depending on the type of interaction and the properties of the stars involved, they can lead to various phenomena, including mass transfer, tidal effects, common envelope evolution, and even stellar mergers.

- ⋆ Mass Transfer: In close binary systems, one star can transfer mass to its companion through different mechanisms. In a Roche lobe overflow scenario, when a star expands beyond its Roche lobe (see Fig. 1.2(c)), gas flows from the expanded star onto its companion. This mass transfer can significantly affect the evolutionary paths of both stars, altering their masses, luminosities, and evolutionary timescales.

- ⋆ Tidal Effects: The tidal gravitational forces between stars in a binary system can induce tidal effects, causing the stars to become tidally distorted. Tidal interactions can lead to the transfer of angular momentum, orbital circularization, and synchronization of the stars' rotations with their orbital motion. These effects can impact the stars' internal structure, rotational velocities, and magnetic activity. It will also affect their apsidal motion, as it will be developed and discussed in this work.

- ⋆ Common Envelope Evolution: In some cases, when a star evolves and expands, its outer envelope can envelop the companion, leading to a common envelope phase. During this phase, the outer envelope of the evolving star and the companion share a common envelope of gas. The interaction between the envelope and the companion can result in orbital energy dissipation and the spiral-in of the companion. Common envelope evolution can lead to binary tightening, orbital shrinkage, and potential mergers or the formation of close binary systems.

- ⋆ Stellar Mergers: In certain cases of extreme interactions, particularly in close binaries, stars can merge, resulting in the formation of a single, more massive star. Stellar mergers can have a significant impact on the properties and evolution of the resulting merged star.

The consequences of these interactions on stellar evolution depend on various factors such as the masses, separation, orbital eccentricity, and initial conditions of the binary system. These interactions can lead to changes in the stars' evolutionary paths, alter their surface abundances, affect their nuclear burning rates, and influence the formation of exotic objects such as cataclysmic variables, X-ray binaries, or even supernovae.

1.1.5 Multiple-star systems

Even if this work focused on binary star systems, it can exist systems of three or more stars that are gravitationally bound to each other. These are called multiple-star systems. They can have various configurations and, as for binary systems, they can exhibit various forms of interaction and dynamics. The gravitational interactions between the stars can lead to orbital changes, mass transfer, stellar collisions, and the exchange of companions. These interactions can significantly impact the evolution and stability of the system, influencing the stellar populations and leading to the formation of exotic objects.

A particular example of a multiple-star system is TYC 7037-89-1, a six-star system, discovered by TESS and announced in January 2021. In Figure 1.5[3] is presented the system configuration. This was the first system where the stars can be observed eclipsing one another, because their planes of rotation point approximately towards the Earth.

[3] From https://universe.nasa.gov/stars/multiple-star-systems/ (10/07/23)

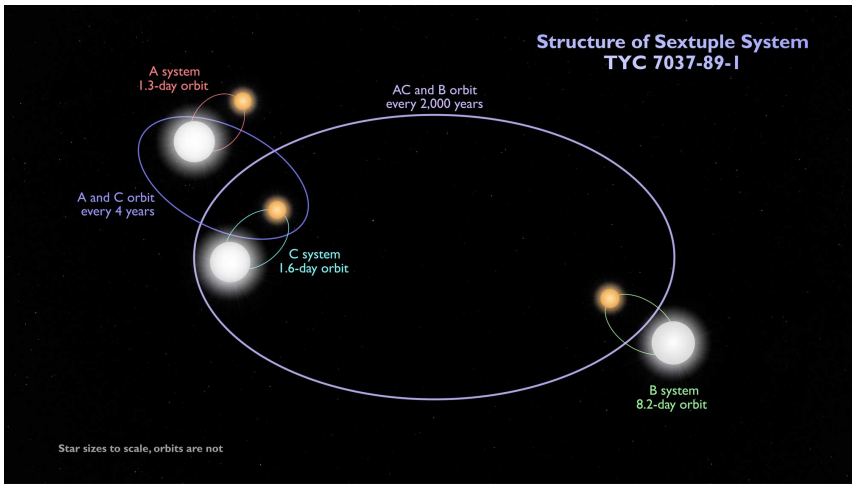

Figure 1.5: This schematic shows the configuration of the sextuple star system TYC 7037-89-1. The inner quadruple is composed of two binaries, A and C, which orbit each other every four years or so. An outer binary, B, orbits the quadruple roughly every 2,000 years. All three pairs are eclipsing binaries. The orbits shown are not to scale. Credit: NASA's Goddard Space Flight Center.

1.1.6 Planets

The formation of planets in binary systems can occur through similar processes as in single-star systems. The protoplanetary disk around the stars can give rise to the formation of planets through core accretion or gravitational instability. However, the presence of two stars can also introduce additional dynamics that can influence planet formation, such as perturbations from stellar companions or different disk structures.

It exists different types of planets depending on their orbits inside the binary system, as illustrated in Figure 1.6.

- ⋆ P-Type Planets: These planets orbit around both stars in a binary system. They orbit the binary center of mass, rather than an individual star. They can have complex and dynamically challenging orbits due to the gravitational interaction between the stars.
- ⋆ S-Type Planets: S-type planets orbit around one of the stars in the binary system at a closer separation. They are similar to planets in single-star systems and form within the circumstellar disk around one of the stars. These planets can experience gravitational interactions with the companion star, affecting their orbits over time.

The presence of two stars in a binary system can significantly affect the dynamics of planets. The gravitational interaction between the stars can result in complex orbital configurations for planets, including stable, unstable, and dynamically evolving orbits. The gravitational tug-of-war between the stars can cause orbital eccentricities and tilts, as well as induce orbital precession. It is also possible that orbital instabilities provoke the ejection of the planet. Known as rogue planets, they are not bound anymore to the binary system and

roam through space as free-floating objects.

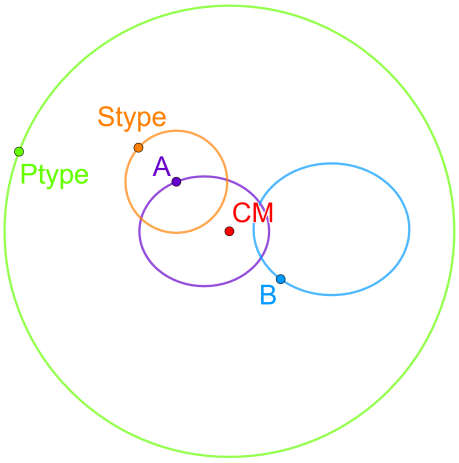

Figure 1.6: Simplified illustration of orbits of planets in a binary star system. Both stars are orbiting on their own orbits and their center of mass is presented in red. The orbit of the P-type planet is presented in green, while the S-type is in orange.

The habitability of planets in binary star systems depends on various factors. The amount of stellar radiation received by a planet is influenced by the separation between the stars, their masses, luminosities, and spectral types. Planets in close binary systems may experience strong tidal forces and intense stellar radiation, potentially affecting their climate, atmosphere, and potential for life.

1.2 Objectives and Outline of the current work

In close binary systems, tidal interactions and rotational effects are crucial in influencing stellar evolution through processes like mass transfer and common envelope phases. However, accurately modelling these aspects requires improvements in theoretical models to account for the breaking of spherical symmetry occurring in close binaries. The current models of binary stars rely on the Roche model and the perturbative approach, both of which involve several assumptions about gravitational, tidal, and centrifugal potentials.

The aim of the work is initially to completely develop the perturbative model to see where the simplifications are located and what they will induce as an error on the binary star system. In a second step, this perturbative model will be compared to MoBiDICT [5], a new non-perturbative 3D static model that computes the deformation in binaries. Finally, those results will then be compared to a system already studied, by S. Rosu [6] [7] to assess them.

In Chapter 2, the theoretical developments for the perturbative method, using spherical harmonics, will be done, to determine the apsidal motion in the binary star system. To do so, the Clairaut-Radau equation will be developed. Then, the different potentials, i.e. the mutual gravitational potentials and the centrifugal potential, will be expanded. Finally, from the precedent results, the expression for the apsidal motion will be determined.

Chapter 3 is dedicated to the MoBiDICT's code. An explanation of its capabilities will be given, as well as the preliminary results obtained by L. Fellay.

In Chapter 4 are given the different results obtained using MoBiDICT. First, the different preliminary results explained in the previous section will be assessed using the theoretical results. Then, the simulations will be done using parameters corresponding to the system observed by S. Rosu [6] [7], in order to determine the correspondence between the simulated and observed results.

Finally, in chapter 5 are discussed the obtained results, as well as the different assumptions made for this work.

1.3 Literature review

Tidal deformations in binary star systems have already been studied, either theoretically or using simulations. This section aims to give a general point of view of what has already been done.

Several theoretical works have been conducted to study tidal deformation and apsidal motion in binary star systems.

The study of close binary stars done by Kopal [8] [9] will be mainly used in this work. Kopal investigates the complex interactions in close binary systems, aiming to unravel the underlying dynamics and the effects of tidal forces, mass transfer and apsidal motion. He developed theoretical models and computational methods to comprehend the behaviour of binary stars, providing insight into their internal structure and the mechanisms governing their evolution. To develop those mathematical models, he used a perturbative method, in order to capture the effects of those perturbations on the different variables he had computed.

Tassoul [10] discussed the theoretical modelling of apsidal motion in close binary systems and its significance as a diagnostic tool for understanding the internal structure of stars. It explores the effects of stellar rotation, gravitational and tidal interactions, and general relativity on the apsidal motion rate. Like Kopal before him, he develops mathematical formalisms and equations to calculate the rate of apsidal motion in binary systems. He also compared theoretical prediction with empirical data.

Shibahashi [11] has investigated the effects of stellar rotation on apsidal motion in close binary systems. He explored the influence of rotation-induced deformation on the orbital dynamics and the rate of apsidal motion. He has also developed theoretical models and conducted numerical simulations to study the rotational effects on the apsidal motion. He highlighted the importance of considering the impact of rotation in understanding the behaviour of binary systems.

Claret and Giménez [12] present a practical method for computing the rate of apsidal motion in binary systems. The authors develop an analytical formula that takes into account factors such as stellar structure and general relativity effects. The method provides a straightforward and efficient approach for calculating the apsidal motion rate in close binary systems. In another paper [13], the authors create a grid of synthetic light curves and radial velocities for detached binary systems. The paper focuses on the generation of synthetic observational data using theoretical models of binary stars. These synthetic datasets allow for the study of various properties, including the apsidal motion, in a range of binary systems.

Besides the theoretical work and the numerical simulations that have been reviewed previously, numerical codes specifically dedicated to the study of binary star systems have been developed.

PHOEBE [14] (PHysics Of Eclipsing BinariEs) is a widely-used code for modelling and analyzing the light curves and radial velocity curves of eclipsing binary systems. It includes features to calculate the apsidal motion and other orbital parameters.

The Wilson-Devinney [15] (WD) code is a widely-used program for modelling and analyzing eclipsing binary systems. It allows for the determination of various parameters, including the apsidal motion rate. It can also handle the complexities of eccentric orbits and asynchronous rotation.

Siess & al. [16] developed BINSTAR, a stellar evolution code designed to study low- and intermediate-mass binaries. They take into account the effect of tidal interactions, mass transfer and angular momentum exchange within the system. They validate their code using the calculation made by the Vrije Universiteit Brussel (VUB) group. They also led a study of different masses and metallicities of stars to determine their influence on the evolution of the system.

2

Perturbative model of tidal deformations

This chapter contains the theoretical developments to evaluate the apsidal motion of a binary system of stars, using the perturbative method. This method implies several assumptions on the system to make the calculations, which will be highlighted to understand where the differences with MoBiDICT are coming from. First, an introduction about spheroid and its implications will be done. Then, the system containing both stars will be described. The Clairaut-Radau equation of the system will also be computed, using the spherical harmonics convention. After that, the different potentials will be evaluated. Finally, the apsidal motion will be determined, from the forces acting on the star.

2.1 Spheroid of a celestial body

Let's first consider the equilibrium of an inhomogeneous self-gravitating celestial body, made of incompressible fluid and rotating around a fixed axis passing through its center of mass, as presented in Figure 2.1. A spheroid is a shape a celestial body will take due to its rotation around the $z-$axis, considered as its rotation axis. Keeping only the $l = 2$ component, the outer boundary of the spheroid is approximately given by:

$$r = R_\theta(\theta) = a\left[1 - \frac{2}{3}\epsilon P_2(\cos\theta)\right], \tag{2.1}$$

where ϵ is the ellipticity and $P_2(\cos\theta)$ the 2^{nd} Legendre polynomial, defined as :

$$P_2(x) = \frac{1}{2}\left(3x^2 - 1\right). \tag{2.2}$$

This ellipticity is defined as:

$$\epsilon = \frac{R_e - R_p}{a}, \tag{2.3}$$

where $R_e = a(1 + \epsilon/3)$ is the radius at the equator, $R_p = a(1 - 2\epsilon/3)$ is the radius at the poles

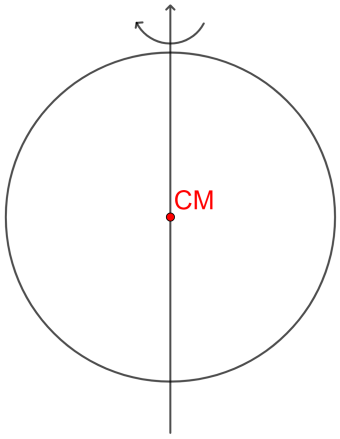

Figure 2.1: Illustration of an inhomogeneous self-gravitating celestial body rotating around a fixed axis passing through its center of mass CM.

(along the rotation axis), and a is the mean radius of the spheroid. In the case of $\epsilon = 0$, the spheroid is reduced to a sphere. However, for $\epsilon < 0$, the spheroid is elongated along its rotation axis and is called prolate, when, for $\epsilon > 0$, the spheroid is squashed and is called oblate. Those two cases are presented in Figure 2.2. Because of the centrifugal forces, the stars in the binary system will be deformed as spheroids.

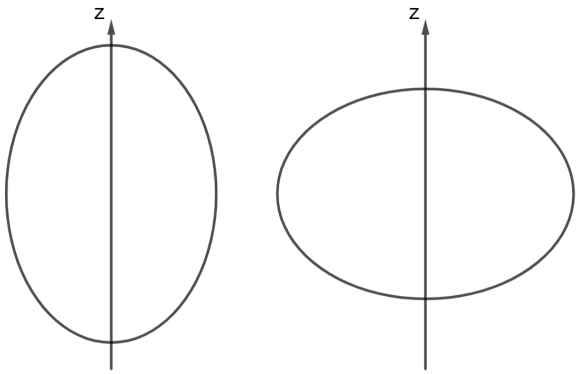

Figure 2.2: Representation of two spheroids: one prolate (left) and one oblate (right).

2.2 Binary stars system

The goal now is to compute the apsidal motion of a star in a binary configuration. In Figure 2.3 is illustrated the coordinate system in which we will work during the theoretical developments. For ease, we work in spherical coordinates, whose symmetry axis coincides with the axis of rotation. The rotation axis of both stars is parallel to the orbit's rotation axis.

For this problem, we will consider an inhomogeneous self-gravitating celestial body, made

of an incompressible fluid, that rotates steadily about some fixed axis passing through its center of mass. As defined before, the shape of the celestial body will be considered as a spheroid, which will be in this case oblate. The hydrostatic equilibrium of this celestial body can be written as:

$$\nabla p = -\rho \nabla U, \tag{2.4}$$

where p is the fluid pressure, ρ the mass density, and $U = \Phi_1 + \Phi_2 + \chi$ is the sum of respectively the gravitational potential from the first star, the gravitational potential from the second star, and the centrifugal potential. It has to be mentioned that the centrifugal force does not always derive from a potential. It is the case for rigid or cylindrical rotations, that is why we will assume a solid body rotation.

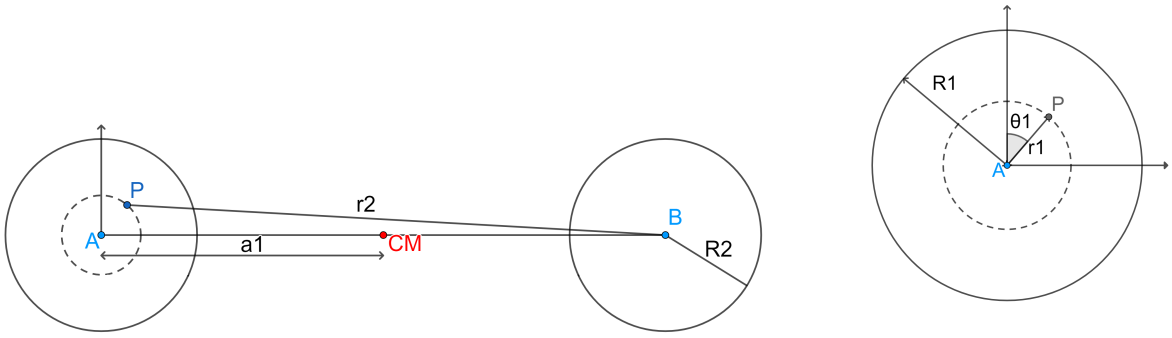

(a) Binary system coordinates

(b) Coordinate system inside a single star

Figure 2.3: Illustration of the coordinate system used for the theoretical developments. A is the primary star, and B is the companion. P is the point at which we observe some parameters. $a1$ is the distance between the center of mass of the system and the center of star A. $R1$ and $R2$ are the mean radius of respectively A and B. $r1$ and $r2$ are the distances from the point P respectively to the center of star A and B. $\theta 1$ is the angle between the point P and the perpendicular axis to the line relying upon both stars' centers, passing through the center of star A.

Taking the curl of equation 2.4, one has

$$\nabla \rho \times \nabla U = 0 \Longleftrightarrow U = U(\rho), \tag{2.5}$$

such that we can deduce that the structure of each star is barotropic, which means that the density and pressure are constant on a given equipotential. For a specified chemical composition, the configuration of stars adopts a thermotropic nature, signifying that the temperature remains also constant on the equipotentials.

As the stars are considered to be spheroids, the radius can be expressed as equation 2.1, such that $r = r(a)$. Then, as the mass density along a spheroid will depend on its mean radius ($\rho = \rho(a)$), the sum of potentials will also depend on a. Assuming that the eccentricity

remains quite small, i.e. that the spheroids are nearly spherical, we will be able to compute the Clairaut-Radau equation, which will give the deformation of the model. The second assumption taking part in the simplification of the perturbation method is then:

$$\epsilon << 1. \tag{2.6}$$

2.3 Clairaut-Radau equation

2.3.1 Development for the density

Using spherical harmonics instead of the Legendre polynomials, r can be developed as:

$$r(\theta,\phi) = a\left[1 + \sum_{l,m\neq 0} \epsilon_{lm}(a)\, Y_l^m(\theta,\phi)\right], \tag{2.7}$$

where Y_l^m is the real spherical harmonic related to the associated Legendre polynomials via the relation: $Y_l^m(\theta,\phi) = \cos(m\phi)\ P_l^m(\cos\theta)$. As $|\epsilon_{lm}| \ll 1$, at first order in ϵ, one has:

$$a(r(\theta,\phi)) = r\left[1 - \sum_{l,m\neq 0} \epsilon_{lm}(r)\, Y_l^m(\theta,\phi)\right] \tag{2.8}$$

The density inside the star can then be developed as follows:

$$\rho(r,\theta,\phi) = \sum_{l,m\neq 0} \rho_{lm}(r)\, Y_l^m(\theta,\phi), \tag{2.9}$$

$$\text{where } \rho_{lm}(r) = \int_\theta \int_\phi \rho(a(r,\theta,\phi))\ Y_l^m(\theta,\phi)\ d\theta d\phi, \tag{2.10}$$

with $\rho(a(r,\theta,\phi))$ the density on the equipotential passing through (r,θ,ϕ). Using the definition of a, given by Eq. 2.8, and Taylor development, one has:

$$\begin{aligned}\rho(a(r,\theta,\phi)) &= \rho(r) + \frac{\partial\rho(r)}{\partial r}\,(r-a) \\ &= \rho(r) + \frac{\partial\rho(r)}{\partial r}\left(r \sum_{l,m\neq 0} \epsilon_{lm}(a)\, Y_l^m(\theta,\phi)\right)\end{aligned} \tag{2.11}$$

One has then:

$$\rho_{lm}(r) = \int_\theta \int_\phi \left[\rho(r) + r\,\frac{\partial\rho(r)}{\partial r} \sum_{l',m'\neq 0} \epsilon_{l'm'}(a)\, Y_{l'}^{m'}(\theta,\phi)\right] Y_l^m(\theta,\phi)\ d\theta d\phi \tag{2.12}$$

The associated Legendre polynomials are orthogonal between them at first order such

that:

$$Y_l^m(\theta,\phi) \times Y_{l'}^{m'}(\theta,\phi) = 0 \quad \text{if} \quad \begin{cases} m \neq m' \\ l \neq l' \end{cases} \tag{2.13}$$

Then, one has the expressions for the density, after integrating on θ and ϕ:

$$\begin{cases} \rho_{l,m\neq 0}(r) = -r\,\dfrac{\partial \rho(r)}{\partial r}\,\epsilon_{lm}(r) \\ \rho_{0,0}(r) = \rho(r) \end{cases} \tag{2.14}$$

The density projected on the equipotential takes then the expression:

$$\begin{cases} \rho_{l,m\neq 0}(a) = -a\,\dfrac{\partial \rho(a)}{\partial a}\,\epsilon_{lm}(a) \\ \rho_{0,0}(a) = \rho(a) \end{cases} \tag{2.15}$$

2.3.2 Poisson Integral

The solution of the Poisson integral will be used to compute the gravitational potential. First, one has spherical coordinates as:

$$\begin{cases} x = r\sin\theta\cos\phi \\ y = r\sin\theta\sin\phi \\ z = r\cos\theta \end{cases} \tag{2.16}$$

The system is axially symmetric considering the deformation along the rotation axis. Then, the density $\rho(\,\underline{r}\,)$ does not depend on ϕ, the azimuthal angle. One can expect that the gravitational potential $\Phi(r,\theta)$ will also not depend on it. This potential has the expression:

$$\Phi(\,\underline{r}\,) = -G\int \frac{\rho(r')}{|r'-r|}\,d^3r' \tag{2.17}$$

where $d^3r' = r'^2\sin\theta' dr' d\theta' d\phi'$ in spherical coordinates. One can then set $\phi = 0$ to estimate the gravitational potential:

$$\Phi(\,\underline{r}\,) = \Phi(r,\theta,\phi=0) = -G\int_0^R\int_0^\pi\int_0^{2\pi} \frac{(r')^2\,\rho(r',\theta')\,\sin\theta'}{\left|\,\underline{r}' - \underline{r}\,\right|}\,d\phi'\,d\theta'\,dr'$$

$$\Longleftrightarrow \Phi(r,\theta) = -2\pi G\int_0^R\int_0^\pi (r')^2\,\rho(r',\theta')\,\sin\theta' < \left|\,\underline{r}' - \underline{r}\,\right|^{-1} > d\theta'\,dr' \tag{2.18}$$

with

$$< \left|\,\underline{r}' - \underline{r}\,\right|^{-1} > \equiv \oint \left|\,\underline{r}' - \underline{r}\,\right|^{-1}\frac{d\phi'}{2\pi} \tag{2.19}$$

This expression can be developed such that:

$$\begin{aligned} \left| \underline{r}' - \underline{r} \right|^{-1} &= \left(r^2 + (r')^2 - 2\, \underline{r}' \cdot \underline{r} \right)^{-1/2} \\ &= \left(r^2 + (r')^2 - 2 r r' F \right)^{-1/2} \end{aligned} \tag{2.20}$$

with $F = \sin\theta \sin\theta' \cos\phi' + \cos\theta' \cos\theta$. The expansion in convergent power series in r'/r, for $r' > r$, is:

$$\left| \underline{r}' - \underline{r} \right|^{-1} = \frac{1}{r} \left[1 + \left(\frac{r'}{r} \right) F + \frac{1}{2} \left(\frac{r'}{r} \right)^2 \left(3F^2 - 1 \right) + \mathcal{O}\left(\frac{r'}{r} \right)^3 \right] \tag{2.21}$$

The mean of the expression of F with respect to ϕ is:

$$< F > = \cos\theta \cos\theta' \tag{2.22}$$

$$\begin{aligned} < F^2 > &= \frac{1}{2} \sin^2\theta \, \sin^2\theta' + \cos^2\theta \, \cos^2\theta' \\ &= \frac{1}{3} + \frac{2}{3} \left(\frac{3}{2} \cos^2\theta - \frac{1}{2} \right) \left(\frac{3}{2} \cos^2\theta' - \frac{1}{2} \right) \end{aligned} \tag{2.23}$$

Then, inserting those expressions in 2.19:

$$< \left| \underline{r}' - \underline{r} \right|^{-1} >= \frac{1}{r} \left[1 + \left(\frac{r'}{r} \right) \cos\theta \cos\theta' + \left(\frac{r'}{r} \right)^2 \left(\frac{3}{2} \cos^2\theta - \frac{1}{2} \right) \left(\frac{3}{2} \cos^2\theta' - \frac{1}{2} \right) + \mathcal{O}\left(\frac{r'}{r} \right)^3 \right] \tag{2.24}$$

One can introduce then the associated Legendre polynomials such that:

$$\Phi(r,\theta) = \sum_{l=0}^{\infty} \sum_{m=-l}^{l} \Phi_{lm}(r)\, Y_l^m(\theta), \tag{2.25}$$

with, as seen before, the associated Legendre polynomials that are orthogonal between them, and

$$\begin{aligned} \Phi_{lm}(r) = & \frac{-2\pi\, G}{r^{l+1}} \int_0^r \int_0^{\pi} (r')^{l+2}\, \rho(r',\theta')\, Y_l^m(\theta')\, \sin\theta'\, d\theta'\, dr' \\ & - 2\pi\, G\, r^l \int_r^R (r')^{1-l}\, \rho(r')\, Y_l^m(\theta')\, \sin\theta'\, d\theta'\, dr' \end{aligned} \tag{2.26}$$

As seen in Eq.2.9, the expression of the density can also be developed with the associated Legendre polynomials, with ρ_{lm} taking the expression:

$$\rho_{lm}(r) = (l + 1/2) \int_0^{\pi} \rho(r,\theta) Y_l^m(\theta)\, \sin\theta\, d\theta. \tag{2.27}$$

Then, one has finally:

$$\begin{aligned}\Phi_{lm}(r) = &\frac{-2\pi\, G}{(l+1/2)\, r^{l+1}} \int_0^r (r')^{l+2}\, \rho_{lm}(r')\, dr' \\ &- \frac{2\pi\, G\, r^l}{l+1/2} \int_r^R (r')^{1-l}\, \rho_{lm}(r')\, dr'\end{aligned} \tag{2.28}$$

2.3.3 Spectral development on equipotential

We want now to develop this expression of the gravitational potential on the equipotential, such that:

$$\Phi_r(r,\theta,\phi) \rightarrow \Phi_a(a,\theta\phi) \tag{2.29}$$

For this, we will expand the expression of Φ such that:

$$\begin{aligned}\Phi_a(a,\theta,\phi) &= \Phi_r(r(a,\theta,\phi),\theta,\phi) \\ &= \Phi_0(r(a,\theta,\phi),\theta,\phi) + \sum_{l,m\neq 0} \Phi_{lm}(r)\, Y_l^m(\theta,\phi) \\ &= \Phi_0(a) + \frac{\partial \Phi_0}{\partial r}(r-a) + \sum_{l,m\neq 0} \underbrace{\Phi_{lm}(a)}_{\text{at first approximation}} \quad Y_l^m(\theta,\phi) \\ &= \Phi_0(a) + \sum_{l,m\neq 0} \left(\Phi_{lm}(a) + a\frac{\partial \Phi_0}{\partial a}\epsilon_{lm}(a)\right) Y_l^m(\theta,\phi) \\ &\text{as} \quad \frac{\partial \Phi_0}{\partial r}(r-a) \approx \frac{\partial \Phi_0}{\partial a}\left[a\, \epsilon_{lm}(a)\; Y_l^m(\theta,\phi)\right]\end{aligned} \tag{2.30}$$

Moreover, one has $\Phi_a = \Phi_0'(a) + \sum_{l,m\neq 0} \Phi_{lm}'(a) Y_l^m(\theta,\phi)$, so that:

$$\begin{cases} \Phi_0'(a) = \Phi_0(a) \\ \Phi_{lm}'(a) = \Phi_{lm}(a) + a\, \dfrac{\partial \Phi_0}{\partial a}\, \epsilon_{lm}(a) = \Phi_{lm}(a) + \dfrac{G\, m(a)}{a}\, \epsilon_{lm}(a) \quad \text{for } l \neq 0 \end{cases} \tag{2.31}$$

As $\partial \Phi_0(a)/\partial a = G\, m(a)/a^2$ by definition of the gravitational potential.

2.3.4 Insertion of the expression of density on equipotential

From Eq. 2.15, one has the expression of ρ_{lm} on the equipotential. One wants then to insert it into Eq. 2.28. For this, one can develop separately, by parts:

$$\begin{aligned}\int_0^a (a')^{l+2}\rho_{lm}da' &= -\int_0^a (a')^{l+3}\frac{d\rho}{da}\epsilon_{lm}(a')da' \\ &= -\left[(a')^{l+3}\rho\,\epsilon_{lm}\right]_0^a + \int_0^a \rho\, d\left(\epsilon_{lm}\,(a')^{l+3}\right) \qquad (2.32)\\ \int_a^R (a')^{1-l}\rho_{lm}da' &= -\int_a^R (a')^{2-l}\frac{d\rho}{da}\epsilon_{lm}(a')da' \\ &= -\left[(a')^{2-l}\rho\,\epsilon_{lm}\right]_a^R + \int_a^R \rho\, d\left(\epsilon_{lm}\,(a')^{2-l}\right) \qquad (2.33)\end{aligned}$$

Then, one can insert in the expression of the potential as follow:

$$\begin{aligned}\Phi_{lm}(a) =& \frac{-2\pi\,G}{(l+1/2)}\,a^{-l-1}\left\{-\left[(a')^{l+3}\rho\,\epsilon_{lm}\right]_0^a + \int_0^a \rho\, d\left(\epsilon_{lm}\,(a')^{l+3}\right)\right\} \\ &- \frac{2\pi\,G}{l+1/2}a^l\left\{-\left[(a')^{2-l}\rho\,\epsilon_{lm}\right]_a^R + \int_a^R \rho\, d\left(\epsilon_{lm}\,(a')^{2-l}\right)\right\} \\ =& \frac{-2\pi\,G}{(l+1/2)}\left\{\cancel{-a^2\rho\epsilon_{lm}} + a^{-l-1}\int_0^a \rho\, d\left(\epsilon_{lm}\,(a')^{l+3}\right)\right. \\ &\left. + \cancel{a^2\rho\epsilon_{lm}} + a^l\int_a^R \rho\, d\left(\epsilon_{lm}\,(a')^{2-l}\right)\right\}\end{aligned}$$

Because for $R >> \epsilon_{lm}$, $\epsilon_{lm}(R) \sim 0$. The final expression for the potential, after simplifications, is then:

$$\Phi_{lm}(a) = \frac{-2\pi\,G}{(l+1/2)}\left\{a^{-l-1}\int_0^a \rho\, d\left(\epsilon_{lm}\,(a')^{l+3}\right) + a^l\int_a^R \rho\, d\left(\epsilon_{lm}\,(a')^{2-l}\right)\right\} \qquad (2.34)$$

2.3.5 Total potential

The total potential will be constant along the equipotential, by definition. This total potential is the sum of the potentials acting on the body, i.e.

$$\Phi_{\text{tot}} = \Phi_1 + \Phi_2 + \Phi_c \qquad (2.35)$$

where Φ_1 is the potential generated by the first star, Φ_2 by the second, and Φ_c results from the centrifugal forces. For $l, m \neq 0$, one has:

$$\Phi_{\text{tot},lm} = \Phi'_{1,lm} + \Phi'_{2,lm} + \Phi'_{c,lm} \qquad (2.36)$$

Taking into account Eq. 2.31, one can multiply Eq. 2.34 by $a^{l+1}/4\pi G$ such that:

$$\frac{-1}{2l+1}\left\{\int_0^a \rho\, d\left(\epsilon_{lm}\,(a')^{l+3}\right) + a^{2l+1}\int_a^R \rho\, d\left(\epsilon_{lm}\,(a')^{2-l}\right)\right\} + \frac{a^l\, m(a)}{4\pi}\epsilon_{lm} + \frac{a^{l+1}}{4\pi G}\left(\Phi_{2,lm}+\Phi_{c,lm}\right) = 0 \tag{2.37}$$

Considering that at first approximation, $\Phi'_{2,lm}+\Phi'_{c,lm} \approx \Phi_{2,lm}+\Phi_{c,lm}$

2.3.6 Derivation

To obtain the Clairau-Radau equation for this system, one has first to derive Eq. 2.37 with respect to a, such that:

$$\begin{aligned}\frac{d}{da}\left[\frac{-1}{2l+1}\int_0^a \rho\, d\left(\epsilon_{lm}\,(a')^{l+3}\right)\right] &= \frac{-1}{2l+1}\rho\frac{d\left(\epsilon_{lm}\,(a')^{l+3}\right)}{da} \\ &= \frac{-1}{2l+1}\left(\rho\frac{d\epsilon}{da}a^{l+3} + \rho\epsilon\,(l+3)\,a^{l+2}\right) \\ &= \frac{-a^{l+2}}{2l+1}\left(\rho\frac{d\epsilon}{da}a + \rho\epsilon\,(l+3)\right)\end{aligned} \tag{2.38}$$

$$\begin{aligned}\frac{d}{da}\left[\frac{-1}{2l+1}\,a^{2l+1}\int_a^R \rho\, d\left(\epsilon_{lm}\,(a')^{2-l}\right)\right] &= \frac{-(2l+1)}{2l+1}a^{2l}\int_a^R \rho\, d\left(\epsilon_{lm}\,(a')^{2-l}\right) + \frac{1}{2l+1}a^{2l+1}\rho\frac{d(\epsilon\, a^{2-l})}{da} \\ &= -a^{2l}\int_a^R \rho\, d\left(\epsilon_{lm}\,(a')^{2-l}\right) + \frac{a^{2l+1}}{2l+1}\left(\rho\frac{d\epsilon}{da}\,a^{2-l} + \rho\epsilon(2-l)a^{1-l}\right) \\ &= -a^{2l}\int_a^R \rho\, d\left(\epsilon_{lm}\,(a')^{2-l}\right) + \frac{a^{l+2}}{2l+1}\left(\rho\frac{d\epsilon}{da}\,a + \rho\epsilon(2-l)\right)\end{aligned} \tag{2.39}$$

$$\begin{aligned}\frac{d}{da}\left[\frac{a^l\, m(a)}{4\pi}\epsilon\right] &= \frac{1}{4\pi}\frac{d}{da}\left[a^l\, m(a)\,\epsilon\right] \\ &= \frac{1}{4\pi}\left(l\,a^{l-1}\,m\,\epsilon + a^l\frac{dm}{da}\epsilon + a^l\,m\frac{d\epsilon}{da}\right) \\ &= \frac{1}{4\pi}a^{l-1}\left(l\,m\,\epsilon + a\frac{dm}{da}\epsilon + a\,m\frac{d\epsilon}{da}\right) \\ &= a^{l-1}\left(\frac{l\,m\,\epsilon}{4\pi} + \rho\,a^3\,\epsilon + \frac{a\,m}{4\pi}\frac{d\epsilon}{da}\right) \quad \text{as } m = \frac{4\pi}{3}\int_0^a \rho a'^2 da'\end{aligned} \tag{2.40}$$

$$\frac{d}{da}\left[\frac{a^{l+1}}{4\pi\,G}\left(\Phi_{2,lm}+\Phi_{c,lm}\right)\right] = \frac{1}{4\pi G}\frac{d}{da}\left[a^{l+1}\left(\Phi_{2,lm}+\Phi_{c,lm}\right)\right] \tag{2.41}$$

Putting everything together, one has:

$$\begin{aligned}
\frac{d}{da}\left[\text{Eq. 2.37}\right] = & \frac{-a^{l+2}}{2l+1}\left(\cancel{\rho\frac{d\epsilon}{da}}a + \rho\epsilon\,(l+3)\right) \\
& - a^{2l}\int_a^R \rho\, d\left(\epsilon_{lm}\,(a')^{2-l}\right) + \frac{a^{l+2}}{2l+1}\left(\cancel{\rho\frac{d\epsilon}{da}}a + \rho\epsilon(2-l)\right) \\
& + a^{l-1}\frac{m}{4\pi}\left(l\,\epsilon + a\,\frac{d\epsilon}{da}\right) + \rho\, a^{l+2}\,\epsilon + \frac{1}{4\pi G}\frac{d}{da}\left[a^{l+1}\left(\Phi_{2,lm}+\Phi_{c,lm}\right)\right] \\
= & -a^{2l}\int_a^R \rho\, d\left(\epsilon_{lm}\,(a')^{2-l}\right) + a^{l-1}\frac{m}{4\pi}\left(l\,\epsilon + a\,\frac{d\epsilon}{da}\right) \\
& + \frac{1}{4\pi G}\frac{d}{da}\left[a^{l+1}\left(\Phi_{2,lm}+\Phi_{c,lm}\right)\right] \\
& + a^{l+2}\underbrace{\left(\frac{-\rho\epsilon(l+3)}{2l+1} + \frac{\rho\epsilon(2-l)}{2l+1} + \rho\epsilon\right)}_{=0} = 0
\end{aligned} \tag{2.42}$$

The mean value of the density is given by $\overline{\rho} = 3\ m/4\pi\ a^3 \longleftrightarrow m\ a^{l-1}/4\pi = \overline{\rho}\ a^{l+2}/3$. Replacing this expression in Eq. 2.42, one has:

$$-a^{2l}\int_a^R \rho\, d\left(\epsilon_{lm}\,(a')^{2-l}\right) + \frac{1}{3}\overline{\rho}a^{l+2}\left(l\,\epsilon + a\,\frac{d\epsilon}{da}\right) + \frac{1}{4\pi G}\frac{d}{da}\left[a^{l+1}\left(\Phi_{2,lm}+\Phi_{c,lm}\right)\right] = 0 \tag{2.43}$$

Dividing this equation by a^{2l} and then derivating with respect to a, one has:

$$\begin{aligned}
\frac{d}{da}\left[-\int_a^R \rho\, d\left(\epsilon_{lm}\,(a')^{2-l}\right)\right] &= \rho\,\frac{d\left(\epsilon_{lm}\,(a')^{2-l}\right)}{da} \\
&= \rho\left((2-l)a^{1-l}\,\epsilon + a^{2-l}\frac{d\epsilon}{da}\right) \\
&= \rho\, a^{1-l}\left((2-l)\,\epsilon + a\frac{d\epsilon}{da}\right)
\end{aligned} \tag{2.44}$$

$$\begin{aligned}
\frac{d}{da}\left[\frac{1}{3}\overline{\rho}a^{-l+2}\left(l\,\epsilon + a\,\frac{d\epsilon}{da}\right)\right] &= \frac{1}{3}\frac{d\,\overline{\rho}}{da}\left(l\,a^{-l+2}\epsilon + a^{-l+3}\,\frac{d\epsilon}{da}\right) \\
&\quad + \frac{1}{3}\overline{\rho}\left[(3-l)a^{2-l}\frac{d\epsilon}{da} + a^{3-l}\frac{d^2\epsilon}{da^2}\right. \\
&\quad \left. + l\,a^{1-l}(2-l)\epsilon + l\,a^{2-l}\frac{d\epsilon}{da}\right] \\
&= \frac{1}{3}\frac{d\,\overline{\rho}}{da}\left(l\,a^{-l+2}\epsilon + a^{-l+3}\,\frac{d\epsilon}{da}\right) \\
&\quad + \frac{1}{3}\overline{\rho}\left(a^{3-l}\frac{d^2\epsilon}{da^2} + 3a^{2-l}\frac{d\epsilon}{da} + l(2-l)a^{1-l}\epsilon\right)
\end{aligned} \tag{2.45}$$

$$\frac{d}{da}\left[\frac{1}{a^{2l}}\frac{1}{4\pi G}\frac{d}{da}\left[a^{l+1}\left(\Phi_{2,lm}+\Phi_{c,lm}\right)\right]\right]=\frac{1}{4\pi G}\frac{d}{da}\left[\frac{1}{a^{2l}}\frac{d}{da}\left[a^{l+1}\left(\Phi_{2,lm}+\Phi_{c,lm}\right)\right]\right] \tag{2.46}$$

Then, adding every term and multiplying by $3a^{l-1}/\overline{\rho}$:

$$\begin{aligned}3\,\frac{\rho}{\overline{\rho}}\left((2-l)\,\epsilon+a\frac{d\epsilon}{da}\right)+\frac{1}{\overline{\rho}}\frac{d\,\overline{\rho}}{da}\left(l\;a\epsilon+a^2\;\frac{d\epsilon}{da}\right)\\ +\left(a^2\frac{d^2\epsilon}{da^2}+3a\frac{d\epsilon}{da}+l(2-l)\epsilon\right)\\ +\underbrace{\frac{3\,a^{l-1}}{4\pi G\,\overline{\rho}}\frac{d}{da}\left[\frac{1}{a^{2l}}\frac{d}{da}\left[a^{l+1}\left(\Phi_{2,lm}+\Phi_{c,lm}\right)\right]\right]}_{\dagger}=0.\end{aligned} \tag{2.47}$$

However, one has the relation:

$$\frac{\rho}{\overline{\rho}}=1+3\frac{a}{\overline{\rho}}\frac{d\overline{\rho}}{da}\quad\rightarrow\quad\frac{1}{\overline{\rho}}\frac{d\overline{\rho}}{da}=\left(\frac{\rho}{\overline{\rho}}-1\right)\frac{3}{a}. \tag{2.48}$$

Simplifying with this expression, we obtain:

$$\begin{aligned}3\,\frac{\rho}{\overline{\rho}}\left((2-l)\,\epsilon+a\frac{d\epsilon}{da}\right)+3\,\frac{\rho}{\overline{\rho}}\left(l\,\epsilon+a\;\frac{d\epsilon}{da}\right)\\ -3\left(l\,\epsilon+a\;\frac{d\epsilon}{da}\right)+\left(a^2\frac{d^2\epsilon}{da^2}+3a\frac{d\epsilon}{da}+l(2-l)\epsilon\right)+\dagger=0.\end{aligned} \tag{2.49}$$

$$\Longleftrightarrow a^2\frac{d^2\epsilon}{da^2}+6\,\frac{\rho}{\overline{\rho}}\left(a\frac{d\epsilon}{da}\epsilon\right)-l(l+1)\epsilon+\dagger=0. \tag{2.50}$$

At first order, the term $\Phi_{2,lm}+\Phi_{c,lm}$ is proportional to a^l if the companion star is treated as a punctual source (see section 2.5). With the derivative inside the term †, the whole term can be neglected.

It is possible to define the structural coefficient by the parameter η_{lm}, such that:

$$\eta=\frac{a}{\epsilon}\;\frac{d\epsilon}{da}, \tag{2.51}$$

where we note η_{lm} as η and ϵ_{lm} as ϵ. One has then:

$$\frac{d\epsilon}{da}=\frac{\eta\epsilon}{a}\quad\text{and}\quad\frac{d^2\epsilon}{da^2}=\left(\frac{d\eta}{da}\;\frac{1}{a}+\frac{\eta(\eta-1)}{a^2}\right)\epsilon. \tag{2.52}$$

We can replace this expression in equation 2.50, taking into account that the term † can

be neglected, so that:

$$\epsilon\, a^2 \left(\frac{d\eta}{da}\,\frac{1}{a} + \frac{\eta(\eta-1)}{a^2}\right) + \frac{3\rho}{\bar{\rho}}\, a \left(\frac{\eta\epsilon}{a}\right) + \frac{3\rho}{\bar{\rho}} l\epsilon - (l+1)\, l\epsilon = 0.$$

Dividing by ϵ, we obtain:

$$a\frac{d\eta}{da} + \eta(\eta-1) + \frac{3\rho}{\bar{\rho}}(\eta+l) - l(l+1) = 0. \tag{2.53}$$

This last equation is known as the Clairaut-Radau equation.

2.4 Potential evaluation inside 1

From equation 2.37, we will be able to compute the expression for the potential inside the first star. One has to divide this equation by a^{2l+1} and derive it with respect to a. Taking into account that $m(a)/4\pi = \int_0^a \rho a'^2 da$:

$$\begin{aligned}
\frac{d}{da}\left[\frac{-1}{2l+1}\frac{1}{a^{2l+1}}\int_0^a \rho\, d\left(\epsilon_{lm}\,(a')^{l+3}\right)\right] &= \frac{1}{a^{2l+2}}\int_0^a \rho\, d\left(\epsilon_{lm}\,(a')^{l+3}\right) \\
&\quad + \frac{-1}{2l+1}\frac{1}{a^{2l+1}}\rho\frac{d(\epsilon\, a^{l+3})}{da} \\
&= \frac{1}{a^{2l+2}}\int_0^a \rho\, d\left(\epsilon_{lm}\,(a')^{l+3}\right) \\
&\quad + \frac{-1}{2l+1}\frac{1}{a^{2l+1}}\rho\left(a^{l+3}\frac{d\epsilon}{da} + \epsilon(l+3)a^{l+2}\right).
\end{aligned} \tag{2.54}$$

$$\begin{aligned}
\frac{d}{da}\left[\frac{-1}{2l+1}\int_a^R \rho\, d\left(\epsilon_{lm}\,(a')^{2-l}\right)\right] &= \frac{1}{2l+1}\rho\frac{d(\epsilon a^{2-l})}{da} \\
&= \frac{1}{2l+1}\rho\left(a^{2-l}\frac{d\epsilon}{da} + \epsilon(2-l)a^{1-l}\right).
\end{aligned} \tag{2.55}$$

$$\begin{aligned}
\frac{d}{da}\left[\frac{a^{-l-1}\, m(a)}{4\pi}\epsilon_{lm}\right] &= -\frac{m(a)\epsilon}{4\pi}(l+1)a^{-l-2} + \frac{a^{-l-1}\epsilon}{4\pi}\frac{d(m(a))}{da} + \frac{a^{-l-1}m(a)}{4\pi}\frac{d\epsilon}{da} \\
&= -\frac{\epsilon}{a^{l+2}}(l+1)\int_0^a \rho a'^2 da + \frac{\epsilon}{a^{l+1}}\frac{d}{da}\left(\frac{m(a)}{4\pi}\right) + \frac{1}{a^{l+1}}\frac{d\epsilon}{da}\int_0^a \rho a'^2 da \\
&= -\frac{\epsilon}{a^{l+2}}(l+1)\int_0^a \rho a'^2 da + \frac{\epsilon}{a^{l+2}}\rho a^3 + \frac{\epsilon}{a^{l+2}}\frac{a}{\epsilon}\frac{d\epsilon}{da}\int_0^a \rho a'^2 da \\
&= \frac{\epsilon}{a^{l+2}}(\eta - 1 - l)\int_0^a \rho a'^2 da + a^{1-l}\rho\epsilon.
\end{aligned} \tag{2.56}$$

$$\frac{d}{da}\left[\frac{a^{l+1}}{4\pi G}\left(\Phi_{2,lm}+\Phi_{c,lm}\right)\right] = \frac{1}{4\pi G}\frac{d}{da}\left[\frac{\Phi_{2,lm}+\Phi_{c,lm}}{a^l}\right] \sim 0, \tag{2.57}$$

as we consider at first approximation that both potentials are proportional to a^l. Regrouping those results together, one has:

$$\begin{aligned}\frac{d}{da}[a^{-2l-1}(\text{Eq 2.37})] &= \frac{1}{a^{2l+2}}\int_0^a \rho\, d\left(\epsilon_{lm}\,(a')^{l+3}\right) + \frac{-1}{2l+1}\frac{1}{a^{2l+1}}\rho\left(a^{l+3}\frac{d\epsilon}{da}+\epsilon(l+3)a^{l+2}\right)\\ &\quad + \frac{1}{2l+1}\rho\left(a^{2-l}\frac{d\epsilon}{da}+\epsilon(2-l)a^{1-l}\right) + \frac{\epsilon}{a^{l+2}}(\eta-1-l)\int_0^a \rho a'^2 da + a^{1-l}\rho\epsilon\\ &= \frac{1}{a^{2l+2}}\int_0^a \rho\, d\left(\epsilon_{lm}\,(a')^{l+3}\right) + \frac{\epsilon}{a^{l+2}}(\eta-1-l)\int_0^a \rho a'^2 da = 0.\end{aligned} \tag{2.58}$$

One can then multiply this equation by $2\pi G\, a^{l+1}/(l+1/2)$ to replace the integrals in equation 2.34. Such calculations will give an expression for the potential inside the first star as:

$$\Phi_{1,lm}(a) = \frac{2\pi\, G}{(l+1/2)}\left\{\frac{\epsilon\, m(a)}{4\pi a}(\eta-1-l) - a^l\int_a^R \rho\, d\left(\epsilon_{lm}\,(a')^{2-l}\right)\right\}. \tag{2.59}$$

Keep going with the first-order approximation, and considering that we are on the surface of the star, where $a = R$:

$$\Phi_{1,lm}(R) \simeq \frac{\epsilon\, GM}{(2l+1)R}(\eta-1-l). \tag{2.60}$$

From equation 2.42 on the surface, one has:

$$\epsilon\, GM = -(2l+1)\frac{\Phi_{2,lm}+\Phi_{c,lm}}{\eta+l}R, \tag{2.61}$$

where all variables that depend on a, i.e. ϵ, η and both potential, are also evaluated at the surface of the star. Inserting this result in the previous equation, one has:

$$\Phi_{1,lm}(R) = \underbrace{\frac{1+l-\eta}{\eta+l}}_{2k_{l,1}}\left(\Phi_{2,lm}+\Phi_{c,lm}\right). \tag{2.62}$$

The first factor can be defined as $k_{l,1}$ corresponds to the apsidal motion's constant.

2.5 Potential generated by 2 inside 1

As it has been developed and explained by Kopal [8] [9], the second star can be treated as a punctual source by the first star. Then, the potential generated by the second star inside

the first one can be developed as:

$$\begin{aligned}\Phi_2(r_1,\theta_1,\phi_1) &= -\frac{G\,M_2}{r_2} \\ &= -\frac{G\,M_2}{a}\sum_l \left(\frac{r_1}{a}\right)^l P_l(\lambda),\end{aligned} \tag{2.63}$$

where λ is defined as $\lambda = \cos\phi_1 \sin\theta_1$.

2.6 Centrifugal potential

In a non-synchronous case, the centrifugal potential can be computed as the sum of the contribution from the rotation of the star around its center, and the contribution from the rotation of the star around the center of mass of the system. In Figure 2.4 is illustrated this configuration. The vectors a_0 and a_{R1} are the centripetal acceleration vectors, respectively given by the expressions:

$$\vec{a}_0 = \Omega_0^2 a_1 \mathbf{e_x} = \nabla\left(\Omega_0^2 a_1 x_1\right), \tag{2.64}$$

$$\vec{a}_{R1} = -\Omega_{R1}\, s\mathbf{e_s} = \nabla\left(-\Omega_{R1}^2 \frac{x^2+y^2}{2}\right). \tag{2.65}$$

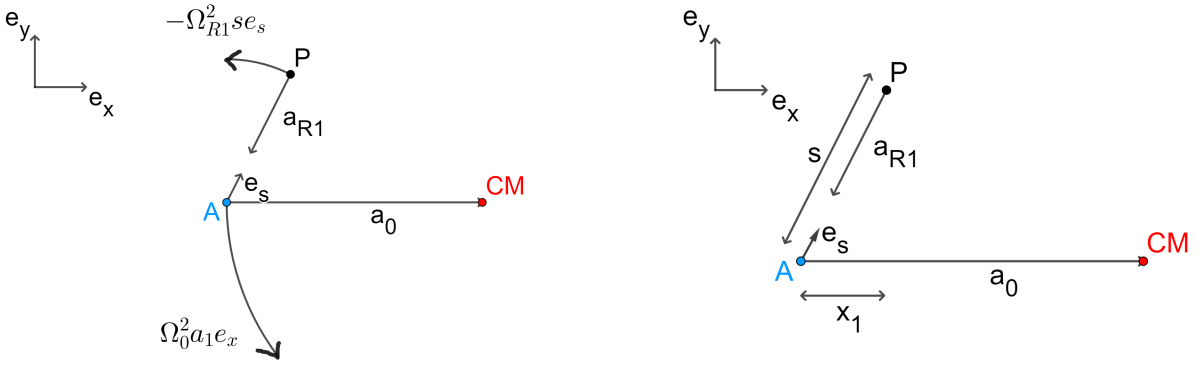

(a) (b)

Figure 2.4: Illustration of the rotations present in the binary system for the primary star. a_{R1} is the vector direction of the rotation with respect to the center of the star. a_0 is the vector direction of the rotation with respect to the center of mass (CM) of the system. Ω_{R1} and Ω_0 are respectively the angular rotational velocities of the rotation around the star's center and the rotation around CM. $s^2 = x_1^2 + y_1^2$ is the distance between the point P and the center of the star A, e_s is its directional vector. x_1 and y_1 are the coordinate of the point P following the coordinate system shown on the figure.

The total centrifugal potential can be then computed as:

$$\Phi_{1,c} = \Omega_0^2 a_1 x_1 - \frac{1}{2}\Omega_{R1}^2 (x_1^2 + y_1^2). \tag{2.66}$$

One can put $\lambda = \cos\phi_1 \sin\theta_1 = x_1/r_1$ and $\nu = \cos\theta_1 = z/r_1$. Then, one has:

$$x_1 = r_1 \, P_1(\lambda), \tag{2.67}$$

$$x_1^2 + y_1^2 = r_1^2 - z^2 = \frac{2}{3} r_1^2 - \frac{2}{3} r_1 \, P_2(\nu). \tag{2.68}$$

The centrifugal potential is then re-expressed as:

$$\begin{aligned} \Phi_{1,c} &= \Omega_0^2 a_1 r_1 \, P_1(\lambda) - \frac{\Omega_{R1}^2}{3} r_1^2 + \frac{\Omega_{R1}^2}{3} r_1 \, P_2(\nu), \\ &= \frac{G\,M_2}{a} \frac{r_1}{a} \, P_1(\lambda) - \frac{\Omega_{R1}^2}{3} r_1^2 + \frac{\Omega_{R1}^2}{3} r_1 \, P_2(\nu). \end{aligned} \tag{2.69}$$

This last step corresponds to the application of Kepler's law.

2.7 Potential inside 1

Now that the last unknowns have been computed, we can come back to the expression of the potential inside 1, in equation 2.62, and replace the expressions obtained for $\Phi_{2,lm}$ and $\Phi_{c,lm}$:

$$\Phi_1(R_1, \lambda, \nu) = \Phi_{1,0} + 2k_{2,1} \left(-\frac{G\,M_2}{a} P_1(\lambda) + \frac{\Omega_{R1}^2 a^2}{3} P_2(\nu) \right) \left(\frac{R_1}{a} \right)^2. \tag{2.70}$$

Similarly, one has the expression for the potential inside the second star:

$$\Phi_2(R_2, \lambda_2, \nu_2) = \Phi_{2,0} + 2k_{2,2} \left(-\frac{G\,M_1}{a} P_1(\lambda_2) + \frac{\Omega_{R2}^2 a^2}{3} P_2(\nu_2) \right) \left(\frac{R_2}{a} \right)^2. \tag{2.71}$$

2.8 Influence of 2 on 1, itself influenced by the deformation of 1

From Kopal's developments [9][1], one has the following expressions:

$$\left(\frac{R}{r_2}\right)^3 = 1 + 3\frac{r}{R}P_1(\lambda) + \frac{r^2}{R^2}\left(5\,P_2(\lambda) + 1\right) + ... \tag{2.72}$$

$$P_2(\lambda_2) = 1 + \frac{r^2}{R^2}\left(P_2(\lambda) - 1\right) + ... \tag{2.73}$$

$$\text{For } j > 2 \rightarrow P_j(\lambda_2) = 1. \tag{2.74}$$

One has also the associated Legendre polynomials:

$$P_2(\lambda) = \frac{1}{4}Y_2^2 - \frac{1}{2}Y_2^0, \tag{2.75}$$

$$P_2(\cos\theta) = Y_2^0. \tag{2.76}$$

For $l = 2$, with $m = 0$ and $m = 2$, the potential in the second star can be estimated as, by replacing $k_{2,2}$ by its expression:

$$\Phi_{22}^0 = \frac{3-\eta_2}{\eta_2+2}\left(\frac{1}{2} + \frac{1}{3}\frac{M}{M_1}\right)\frac{G\,M_1}{a}\left(\frac{R_2}{a}\right)^5\left(\frac{a}{r_2}\right)^3, \tag{2.77}$$

$$\Phi_{22}^2 = -\frac{3-\eta_2}{\eta_2+2}\frac{1}{4}\frac{G\,M_1}{a}\left(\frac{R_2}{a}\right)^5\left(\frac{a}{r_2}\right)^3 \tag{2.78}$$

$$\tag{2.79}$$

Replacing with the expressions given by Kopal, and neglecting the higher order terms, one has:

$$\begin{aligned}\Phi_2(r_2,\theta_2,\phi_2) &= \Phi_{22}^0(r_2)\,Y_2^0(\theta_2,\phi_2) + \Phi_{22}^2(r_2)\,Y_2^2(\theta_2,\phi_2)\\ &= \underbrace{\frac{3-\eta_2}{\eta_2+2}\,\frac{G\,M_1}{a}\left(\frac{R_2}{a}\right)^5}_{\mathrm{X}}\left(\frac{a}{r_2}\right)^3\left[\left(\frac{1}{2}+\frac{1}{3}\frac{M}{M_1}\right)Y_0^2 - \frac{1}{4}Y_2^2\right]\\ &= \mathrm{X}\left(\frac{a}{r_2}\right)^3\left[-P_2(\lambda_2) + \frac{1}{3}\frac{M}{M_1}P_2(\cos\theta_2)\right]\end{aligned} \tag{2.80}$$

One can then develop:

$$\begin{aligned}P_2(\lambda_2)\left(\frac{a}{r_2}\right)^3 &\simeq \left[1 + \left(\frac{R_1}{a}\right)^2\left(P_2(\lambda) - 1\right)\right]\left[1 + \frac{3R_1}{a}P_1(\lambda) + \left(\frac{R_1}{a}\right)^2\left(5P_2(\lambda)+1\right)\right],\\ &\simeq 1 + \frac{3R_1}{a}P_1(\lambda) + 6\left(\frac{R_1}{a}\right)^2 P_2(\lambda) + \mathcal{O}\left(\frac{R_1}{a}\right)^3.\end{aligned} \tag{2.81}$$

[1] Equations 3.8, 3.9 and 3.10, p.38

$$\begin{aligned} P_2(\cos\theta_2) &= \frac{1}{2}\left(3\frac{z^2}{r_2^2}-1\right), \\ &= \frac{1}{2}\left(3\frac{z^2}{a^2}-1\right)+\mathcal{O}\left(\frac{R_1}{a}\right)^3, \\ &\simeq \frac{3}{2}\left(\frac{R_1}{a}\right)^2\cos^2\theta_1-\frac{1}{2}, \\ &\simeq \left(\frac{R_1}{a}\right)^2 P_2(\cos\theta_1)+\frac{1}{2}\left(\frac{R_1}{a}\right)^2-\frac{1}{2}. \end{aligned} \tag{2.82}$$

And finally:

$$P_2(\cos\theta_2)\left(\frac{a}{r_2}\right)^3 = \frac{-1}{2}-\frac{3}{2}\frac{R_1}{a}P_1(\lambda)+\left(\frac{R_1}{a}\right)^2\left[P_2(\cos\theta_1)-\frac{5}{2}P_2(\lambda)\right]+\mathcal{O}\left(\frac{R_1}{a}\right)^3 \tag{2.83}$$

Inserting those expressions into equation 2.80, one has:

$$\begin{aligned} \Phi_2(r_2,\theta_2,\phi_2) = -\mathrm{X}\Bigg[\frac{1}{3}\frac{M}{M_1}\Bigg\{\frac{1}{2}+\frac{3}{2}\frac{R_1}{a}P_1(\lambda)-\frac{R_1^2}{a^2}\left[P_2(\cos\theta_1)-\frac{5}{2}P_2(\lambda)\right]\Bigg\}, \\ +\left\{1+\frac{3R_1}{a}P_1(\lambda)+6\frac{R_1^2}{a^2}P_2(\lambda)\right\}\Bigg]. \end{aligned} \tag{2.84}$$

From Kepler's law, one has:

$$\Omega_{R2}^2 a^2 = \frac{G\,M}{a}\left(\frac{\tilde{P}_0}{P_{R2}}\right)^2, \tag{2.85}$$

where $\tilde{P}_0 = 2\pi/\Omega_0$ is the orbital period and P_{R2} the rotational period of the second star. Developing X, one has the expression for the potential:

$$\begin{aligned} \Phi_2(r_2,\lambda,\nu) =& \Phi_{20}+2k_{22}\left(\frac{R_2}{a}\right)^5\Bigg[\frac{G\,M_1}{a}\left\{1+3\frac{R_1}{a}P_1(\lambda)+6\frac{R_1^2}{a^2}P_2(\lambda)\right\} \\ &+\frac{\Omega_{R2}^2 a^2}{3}\left\{\frac{1}{2}+\frac{3}{2}\frac{R_1}{a}P_1(\lambda)-\frac{R_1^2}{a^2}\left[P_2(\nu)-P_2(\lambda)\right]\right\}\Bigg]. \end{aligned} \tag{2.86}$$

Now, let's see the influence of Φ_2 with respect to r_1:

$$\begin{aligned}\Phi_2(r_1,\lambda,\nu) =& \tilde{\Phi}_{20} - 2k_{22}\left(\frac{R_2}{a}\right)^5 \frac{r_1}{a}\left(\frac{3G\,M_1}{a} + \frac{\Omega_{R2}^2 a^2}{2}\right) P_1(\lambda) \\ & - 2k_{22}\left(\frac{R_2}{a}\right)^5 \left(\frac{r_1}{a}\right)^2 \left[\left(\frac{6G\,M_1}{a} + \frac{5}{6}\Omega_{R2}^2 a^2\right) P_2(\lambda) - \frac{\Omega_{R2}^2 a^2}{3} P_2(\nu)\right], \\ =& \tilde{\Phi}_{20} - 2\mathrm{X}_2 \left[\frac{r_1}{a}\left\{3 + \frac{1}{2}\frac{M}{M_1}\left(\frac{\tilde{P}_0}{P_{R2}}\right)^2\right\}\right. \\ & \left. + \left(\frac{r_1}{a}\right)^2 \left\{6 + \frac{5}{6}\frac{M}{M_1}\left(\frac{\tilde{P}_0}{P_{R2}}\right)^2\right\} P_2(\lambda) - \frac{1}{3}\frac{M}{M_1}\left(\frac{\tilde{P}_0}{P_{R2}}\right)^2 P_2(\nu)\right], \\ =& \tilde{\Phi}_{20} + \tilde{\Phi}_2. \end{aligned} \tag{2.87}$$

The same reasoning can be done for Φ_1.

2.9 Apsidal motion

Now that we have the complete expression for the potential, it is possible to compute the apsidal motion of the system. The apsidal motion is the time variation of the periastron argument, ω, which corresponds to the shift in the position of the apsidal line within the eccentric system. We will begin by calculating the force from the gravitational potential of the second star on the first one that is considered as non-perturbated. One has, for $l = 2$,

$$F_{2'10} = -\int_{V_1} \frac{\partial \Phi_2'}{\partial x_1} \rho_{10}\, dV_1 \simeq -\frac{\partial \Phi_2'}{\partial x_1}(0)\; M \tag{2.88}$$

where the notation "'" stands for perturbated and "0" for non-perturbated. V_1 corresponds to the volume of the first star. The partial derivative is evaluated at the center of the first star. The potential Φ_2 depends on x_1 through the relation $r_1 P_1(\lambda)/a = x_1/a$. Then, the only component that will have a non-zero gradient from the point of view of the first star is the term $l = 1$, such that:

$$\Phi_2' \simeq \tilde{\Phi}_{20} - 2\frac{GM_1}{a} k_{22}\left(\frac{R_2}{a}\right)^5 \frac{x_1}{a}\left(3 + \frac{1}{2}\frac{M}{M_1}\left(\frac{\tilde{P}_0}{P_{R2}}\right)^2\right), \tag{2.89}$$

$$\rightarrow \frac{\partial \Phi_2'}{\partial x_1}(0) M_1 \simeq 2\frac{GM_1^2}{a^2} k_{22}\left(\frac{R_2}{a}\right)^5 \left(3 + \frac{1}{2}\frac{M}{M_1}\left(\frac{\tilde{P}_0}{P_{R2}}\right)^2\right). \tag{2.90}$$

On another side, we can consider the relative acceleration inside the system as:

$$\ddot{\vec{r}} = \left[-\frac{GM}{r^2} + \mathscr{R}\right] \vec{e}_x = \ddot{\vec{r}}_2 - \ddot{\vec{r}}_1, \tag{2.91}$$

where $\mathscr{R}$ is the perturbed acceleration that produces the apsidal motion. From Newton's law,

one has that:

$$\mathscr{R} = \mathscr{R}_{12} - \mathscr{R}_{21} = \frac{F_{12}}{M_2} - \frac{F_{21}}{M_1} = \frac{F_{12}}{\mu} = \frac{-F_{21}}{\mu}, \tag{2.92}$$

where $\mu = M_1 M_2 / M$ is the reduced mass. The densities of both stars are the combination of a non-perturbed and a perturbed term such that $\rho_i = \rho_{i0} + \rho_i'$. Using the same reasoning, the force exerted by the second star on the first can be developed as:

$$F_{21} = F_{2'10} + F_{201'} + F_{2'1'}, \tag{2.93}$$

with the last term negligible at the first order. By action=reaction, one has:

$$F_{201'} = -F_{1'20}. \tag{2.94}$$

One has then:

$$F_{21} = F_{2'10} - F_{1'20}. \tag{2.95}$$

Inserting equations 2.90 and 2.95 inside the expression 2.92:

$$\begin{aligned}\mathscr{R} =& \frac{-F_{21}}{\mu} = \frac{1}{\mu}(F_{1'20} - F_{2'10}) \\ =& -2\frac{GM}{a^2}\left[\frac{1}{q}k_{22}\left(\frac{R_2}{a}\right)^5\left(3 + \frac{1+q}{2}\left(\frac{\tilde{P}_0}{P_{R2}}\right)^2\right)\right. \\ &\left. + k_{21}\left(\frac{R_1}{a}\right)^5 q\left(3 + \frac{1+q}{2q}\left(\frac{\tilde{P}_0}{P_{R2}}\right)^2\right)\right],\end{aligned} \tag{2.96}$$

where $q = M_1 / M_2$ is the mass ratio. It has already been mentioned that the orbital period depends on the separation distance a between both stars. Then, it is possible to define, with A the semi-major axis of the elliptical orbit:

$$\left(\frac{\tilde{P}_0}{P_{R2}}\right)^2 = \frac{4\pi^2 a^3}{GM}\frac{1}{P_R^2} = \left(\frac{a}{A}\right)^3\left(\frac{P_0}{P_{R2}}\right)^2 \tag{2.97}$$

The equation 2.96 becomes then:

$$\begin{aligned}\mathscr{R} =& -2\frac{GM}{A^2}\left[\left\{\frac{k_{22}}{q}3\left(\frac{R_2}{A}\right)^5 + qk_{21}\left(\frac{R_1}{A}\right)^5\right\}\left(\frac{A}{a}\right)^7\right. \\ &\left. + \left\{\frac{k_{22}}{2q}(q+1)\left(\frac{R_2}{A}\right)^5\left(\frac{P_0}{P_{R2}}\right)^2 + \frac{k_{21}}{2}(q+1)\left(\frac{R_1}{A}\right)^5\left(\frac{P_0}{P_{R1}}\right)^2\right\}\left(\frac{A}{a}\right)^4\right]. \\ =& -\left(\mathscr{R}_{\text{tides}}\left(\frac{A}{a}\right)^7 + \mathscr{R}_c\left(\frac{A}{a}\right)^4\right)\frac{GM}{A^2},\end{aligned} \tag{2.98}$$

where $\mathscr{R}_{\text{tides}}$ is the contribution from the tidal deformations and $\mathscr{R}_{\text{c}}$ the contribution from the centrifugal deformations. According to the Gauss planetary equations, the apsidal mo-

tion rate is given by:

$$\frac{d\bar{\omega}}{dt} = -\frac{\sqrt{1-e^2}}{e}\sqrt{\frac{A}{GM}}\int \frac{\mathscr{R}\cos\theta}{P_0}dt. \tag{2.99}$$

$$\Longleftrightarrow \frac{d\bar{\omega}}{dt} = -\frac{\sqrt{1-e^2}}{e}\sqrt{\frac{A}{GM}} < \mathscr{R}\cos\theta > . \tag{2.100}$$

We want to compute the mean value $< \mathscr{R}\cos\theta >$:

$$\frac{1}{P_0}\int_0^{P_0}\left(\frac{A}{a}\right)^4 \cos\theta dt = \mathrm{X}_0^{-4,1} = e(1-e^2)^{-5/2}, \tag{2.101}$$

$$\frac{1}{P_0}\int_0^{P_0}\left(\frac{A}{a}\right)^7 \cos\theta dt = \mathrm{X}_0^{-7,1} = \frac{5}{2}e(1-e^2)^{-11/2}\left(1+\frac{3}{2}e^2+\frac{1}{8}e^4\right), \tag{2.102}$$

where the $X_k^{n,m}$ coefficients are the so-called Hansen coefficients, given by the expression:

$$X_0^{n,m}(e) = \frac{1}{P_0}\int_0^{P_0}\left(\frac{r}{a}\right)^n \cos(m\theta)\, dt. \tag{2.103}$$

Then, one will have, from equation 2.98:

$$< \mathscr{R}\cos\theta > = -\left(\mathscr{R}_{\text{tides}}\mathrm{X}_0^{-7,1} + \mathscr{R}_c\mathrm{X}_0^{-4,1}\right)\frac{GM}{A^2} \tag{2.104}$$

The apsidal motion inside the binary system is then given by:

$$\begin{aligned}\frac{d\bar{\omega}}{dt} =& \frac{\sqrt{1-e^2}}{e}\sqrt{\frac{GM}{A^3}}\left(\mathscr{R}_{\text{tides}}\mathrm{X}_0^{-7,1} + \mathscr{R}_c\mathrm{X}_0^{-4,1}\right)\\ =& \frac{2\pi}{P_0}\left[15f(e)\left\{\left(\frac{R_1}{A}\right)^5 q k_{21} + \left(\frac{R_2}{A}\right)^5 \frac{k_{22}}{q}\right\}\right.\\ &\left. + g(e)\left\{k_{21}(1+q)\left(\frac{R_1}{A}\right)^5\left(\frac{P_0}{P_{R1}}\right)^2 + k_{22}\frac{1+q}{q}\left(\frac{R_2}{A}\right)^5\left(\frac{P_0}{P_{R2}}\right)^2\right\}\right],\end{aligned} \tag{2.105}$$

where $f(e)$ and $g(e)$ are defined as:

$$f(e) = \left(1+\frac{3}{2}e^2+\frac{1}{8}e^4\right)/(1-e^2)^5 \tag{2.106}$$

$$g(e) = 1/(1-e^2)^2 \tag{2.107}$$

Those theoretical developments finally gave us an expression for the apsidal motion rate inside the binary system. Several assumptions have been made to reach this result:

- ⋆ Solid body rotation, such that the centrifugal force derives from a potential.
- ⋆ Small eccentricity so that the spheroids are nearly spherical
- ⋆ Second star is treated as a punctual source by the first one
- ⋆ Several expressions approximate at first order

As it will be explained in the next section, this expression obtained for the perturbative method will be compared to the new non-perturbative method implemented in MoBiDICT.

3

(New) non-perturbative models of tidal deformation

In this chapter will be explained the MoBiDICT code, developed by L. Fellay and M.-A. Dupret [5]. This code is used to simulate binary star systems using a new non-perturbative method. Their results for the comparison of the new model with Roche model and perturbative model are briefly described, and future perspectives expected for the development of the code are explained.

3.1 MoBiDICT

To address the limitations of existing models, L. Fellay and M.-A. Dupret [5] have developed a new non-perturbative method capable of precisely computing the structural deformation of binary systems in three dimensions, even in highly distorted cases. Their new approach was then compared with the Roche and perturbative models for various orbital separations and binary components.

Their computational tool, known as Modelling Binary Deformation Induced by Centrifugal and Tidal forces (MoBiDICT), is implemented in Fortran 95 for computational efficiency. MoBiDICT iteratively solves Poisson's equation, incorporating centrifugal and tidal forces in a non-perturbative manner, i.e. it does not consider the small deformation approximation made by the perturbative method. By not assuming spherically symmetric density distributions, their method considers the redistribution of mass and its impact on the structure and deformation of the stars and their companions. These non-perturbative models provide not only accurate surface quantities but also offer access to the precise 3D structure of each binary system component.

The initial model for the stars' structures inside the binary system is obtained via the "Code Liegeois d'Evolution Stellaire" (CLÉS) developed by R. Scuflaire & al.[18]. Every star can have its own structure such that it is possible to study binary systems with stars of dif-

ferent masses and compositions. They assume that both stars have a rotation axis aligned to the orbital rotational axis, so that the system will have two symmetry plans, which are the orbital plan and the plan including the three rotation axis. Utilizing these two symmetries, it is only needed to describe one-quarter of each star to model the entire 3D system.

CLÉS will give a 1-dimensional density profile, spherically symmetric, of each star i, $\rho_{i,1D}(r,\mu,\phi)$, that will be imposed along a characteristic direction (μ_{crit},ϕ_{crit}) inside each star. This critical direction is chosen to verify the mass conservation, for a mass m_p enclosed under an isobar of pressure p, at each layer of the star, such that:

$$\frac{d\ m_p}{d\ r_p} = 4\pi\rho r_p^2, \tag{3.1}$$

where r_p is the average radius so that $V_p = \frac{4}{3}\pi r_p^3$ is the volume under this isobar. Here, one defines $\mu = \cos(\theta)$, to have simplifications in the computation thanks to the symmetries. To compute the different parameters, a mesh of μ and ϕ based on the Gauss-Legendre quadrature method is employed. After the computation of this initial density profile in 3 dimensions, MoBiDICT will iteratively solve Poisson's equation in 3D space to rigorously calculate the gravitational potential, the deformation and the density in this 3D space.

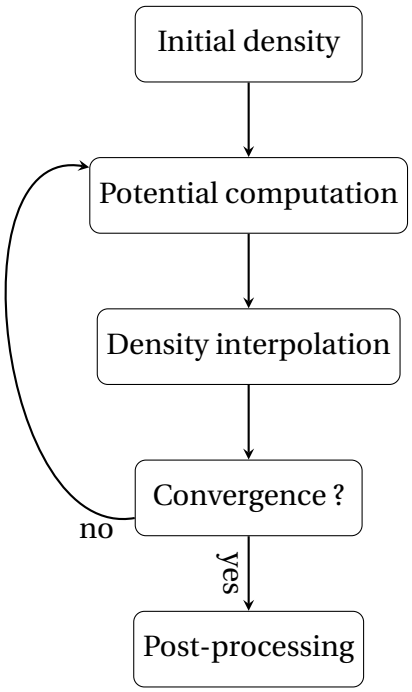

From the initial density profiles, MoBiDICT will compute the total potential inside each star using Poisson's equation for each star. This equation is given as:

$$\frac{1}{r_i^2}\frac{\mathrm{d}}{\mathrm{d}r_i}\left(r_i^2\frac{\mathrm{d}\Phi_{i,\ell}^m}{\mathrm{d}r_i}\right) - \frac{\ell(\ell+1)}{r_i^2}\Phi_{i,\ell}^m = 4\pi G\rho_{i,\ell}^m, \tag{3.2}$$

with the boundary conditions:

$$\begin{cases} \Phi^m_{i,\ell}(0) = 0 \quad \text{if} \quad \ell \neq 0 \\ (\ell+1)\Phi^m_{i,\ell} + r_i \dfrac{\mathrm{d}\Phi^m_{i,\ell}}{\mathrm{d}r_i} = 0 \quad \text{at} \quad r_i = R_{i,0}, \end{cases} \tag{3.3}$$

where $R_{i,0}$ is the radius at the surface of the star i. When integrating this equation, and using the boundary conditions, we can find the expression given by Equation 2.28, developed in the theory part. The total potential of each star is given by the sum:

$$\Phi_{\text{tot}} = \Phi_1 + \Phi_2 + \Phi_{\text{c}}, \tag{3.4}$$

where both Φ_1 and Φ_2 are obtained via Equation 3.2. The centrifugal potential is computed through the expression:

$$\begin{aligned} \Phi_{\text{c}}(r,\mu,\phi) &= -\frac{\Omega_\star^2}{2}\varpi^2(r,\mu,\phi) \\ &= -\frac{\Omega_\star^2}{2}\left[\left(x_{\text{CM}} - r\sin(\theta)\cos(\phi)\right)^2 + (r\sin(\theta)\sin(\phi))^2\right], \end{aligned} \tag{3.5}$$

where $\varpi(r,\mu,\phi)$ is defined as the distance of the element considered to the orbital rotation rate. $\Omega_\star$ is the stellar and orbital rotation rate and x_{CM} is the distance of the star from the centre of mass of the system.

Once the total potential inside each star is computed, the corresponding density will be interpolated. To do so, they take advantage of the barotropic nature of each star's structure, where the density remains constant on equipotential surfaces. Assuming that the density of star i along a given direction μ_{crit} and ϕ_{crit} is the same as the density of the corresponding averaged 1D input model, they establish the functions $\rho_i(\Phi_{i,tot}(r_i,\mu_{crit},\phi_{crit})) = \rho_{i,1D}(r_i)$ for each star. Through simple function composition and interpolation, they estimate the density of the entire star using the total potential at each point of the grid.

Finally, a convergence criterion is defined to end the iteration process. It is guided by the variations in density and gravitational potential between two successive iterations. These variations quantify the contribution of each iteration to the deformation of each point in a star, providing direct control over the convergence of the modelling process. The region where significant deformation is expected to occur is the point nearest to the Lagrangian point L1 in each star i: $(R_{s,i}, \mu = 0, \phi = 0)$. Therefore, if the changes in potential and density at this point become negligible compared to the previous iteration, the entire model is

considered to have converged. The convergence criterion is then, for the j^{th} iteration:

$$\delta\rho^{m}_{i,j,\ell} = \frac{\rho_{i,j}\left(R_{s,i,j},0,0\right) - \rho_{i,j-1}\left(R_{s,i,j-1},0,0\right)}{\rho_{i,j}\left(R_{s,i,j},0,0\right)}, \tag{3.6}$$

or,

$$\delta\Phi^{m}_{i,j,\ell} = \frac{\Phi_{i,j}\left(R_{s,i,j},0,0\right) - \Phi_{i,j-1}\left(R_{s,i,j-1},0,0\right)}{\Phi_{i,j}\left(R_{s,i,j},0,0\right)}. \tag{3.7}$$

They have set the criterion for convergence as $\delta\rho^{m}_{i,j,\ell} < 10^{-8}$ and $\delta\Phi^{m}_{i,j,\ell} < 10^{-8}$ for each star. This choice is based on the normalized precision we achieve with the 1D average input models, which is approximately 10^{-8} on the density. If the model has not converged, the total potential is once again computed using the newly determined density.

To compute the apsidal motion rate, MoBiDICT will use a numerical integration on the orbit. As for the perturbative method, the Gauss planetary equation will be used for a perturbed acceleration along the apsidal line:

$$\frac{d\omega}{dt} = -\frac{\sqrt{1-e^2}}{e}\sqrt{\frac{a}{GM_{tot}}} < \mathscr{R}\cos\varphi >, \tag{3.8}$$

with φ the true anomaly and $< \mathscr{R}\cos\varphi >$ the time average of the perturbed acceleration such that:

$$< \mathscr{R}\cos\varphi >= \frac{\int R\cos\varphi \, dt}{\int dt} \tag{3.9}$$

To derive the apsidal motion of a system in a non-perturbative manner, their approach only requires the computation of the time average of the resulting force. To do so, they took several snapshots of stellar deformations at various points along the binary orbits. Then, from those snapshots, they derive the time-averaged perturbed acceleration by reformulating its expression using the second Kepler's law:

$$dt = \frac{r^2}{na^2\sqrt{1-e^2}}d\varphi, \tag{3.10}$$

where r represents the separation between the stars, expressed using the first Kepler's Law as

$$r = \frac{a(1-e^2)}{1+e\cos(\varphi+)} \tag{3.11}$$

By combining those four latest equations, the apsidal motion rate can be computed as:

$$\frac{d\omega}{dt} = \pi\frac{(1-e^2)}{e}\sqrt{\frac{a}{GM_{tot}}}\int_0^{\pi}\frac{R\cos\varphi}{(1+e\cos(\varphi))^2}d\varphi, \tag{3.12}$$

where the integrals are restricted to half of an orbit due to symmetry considerations. It might be presumed that a substantial number of snapshots taken over an entire orbit is neces-

sary to attain a reasonable level of precision in calculating the apsidal motion. Nevertheless, through our method's implementation, they have observed that utilizing fifteen evenly spaced φ values across half of an orbit is adequate to achieve a relative precision of 10^{-4} to 10^{-5} for the apsidal motion in the vast majority of scenarios.

3.2 Results

3.2.1 Comparison with Roche model

The Roche model is a traditional approach for describing the total potential in a binary system. While this model relies on strong assumptions about the stellar structure, it offers the advantage of providing straightforward analytical expressions for the total potential at any specific point within the binary system, taking into account the gravitational interactions between two point-like bodies and the associated centrifugal potential. Its main advantage lies in the ability to obtain simple analytical expressions for the total potential. However, to derive these expressions, several assumptions are made. Firstly, the stars' orbits are assumed to be circular, and their rotational periods are synchronized with the orbital period. Additionally, for the determination of the potentials, the stars are treated as point-like objects instead of deformed bodies occupying a significant volume. Finally, the Roche model assumes that the stellar density profiles are spherically symmetric, even in highly distorted cases.

The total potential for the Roche model is then given by the expression:

$$\Phi_{\text{tot},1} = \Phi_1 - \frac{GM_2}{r_2} - \frac{\Omega_\star^2}{2}\varpi^2, \tag{3.13}$$

with:

$$\Phi_1 = \int_{R_s}^{r_1} \frac{Gm_1(r)}{r^2} dr - \frac{GM_1}{R_s}. \tag{3.14}$$

It has to be mentioned that this expression, called refined Roche model, is a derivation of the usual Roche model such that it guarantees that the gravitational potential is a solution of Poisson's equation while keeping it untouched outside of the star. The surface corresponds to an equipotential. Therefore, the surface deformation of binary stars is directly influenced by the total potential of the system. In Figure 3.1 are compared the positions of the surfaces predicted by the Roche model and the new model for a $0.2M_\odot$ star with an orbital separation of $2.8R_{1D}$. Here, R_{1D} represents the radius of the 1D spherically symmetric model. The comparison reveals a noticeable difference in surface deformation between both models.

To quantify this difference, a new quantity is introduced: the difference in deformation at the closest point normalized by the deformation between the Roche model and the 1D

input model, given by:

$$\Delta R = \frac{R_{\text{s,MoBiDICT}}(\mu = 0, \phi = 0) - R_{\text{s, Roche}}\,(\mu = 0, \phi = 0)}{R_{\text{s, Roche}}\,(\mu = 0, \phi = 0) - R_{\text{1D}}}. \tag{3.15}$$

For the system shown in Figure 3.1, this factor, denoted as ΔR, is equal to 0.368, indicating that MoBiDICT predicts 36.8% more deformation than the Roche model at the closest surface point to the Lagrangian point L1.

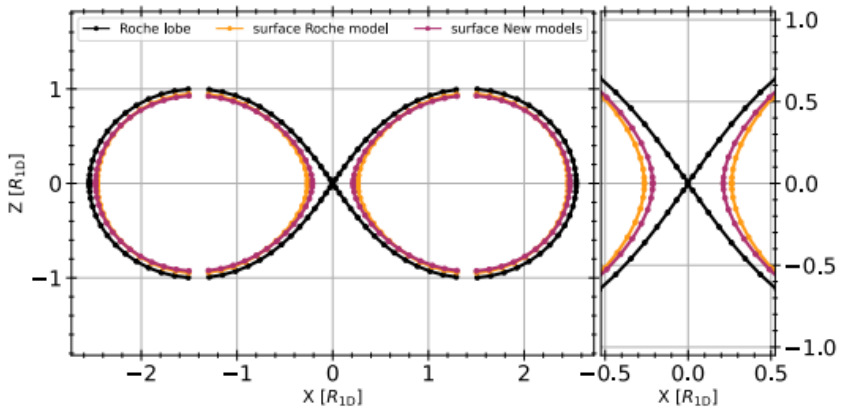

Figure 3.1: Surface deformation of a twin binary system of a $0.2M_{\odot}$ star with an orbital separation of $2.8R_{1D}$. The black curve corresponds to the Roche lobe of the system, the yellow curve is the surface of each star given by the Roche model while the purple curve corresponds to the surface of each star given by the modelling with MoBiDICT. This Figure is directly taken from the article by L. Fellay [5] (Fig.2 p.7).

3.2.2 Comparison with perturbation method

The perturbative models are based on treating the centrifugal and tidal forces as perturbations of the spherical symmetry, considering only the leading terms in the expansion. Both the potentials and densities of these models are projected onto a basis of spherical harmonics, accounting only for the $l = 0$ and $l = 2$ terms.

Figure 3.2 depicts the amplitude hierarchy of gravitational potential spherical terms. As assumed by the perturbative model, the leading order terms are the $l = 0$ and $l = 2$ terms. However, the next most significant term is the dipolar term ($l = 1$), especially outside of the star. Although the perturbative model neglects this $l = 1$ term, it is found to be less than one order of magnitude smaller than the $l = 2$ term. Consequently, the assumption to neglect the $l = 1$ term is not justified for the perturbative models in highly distorted cases. The next-order terms ($l = 3, 4$) have similar amplitudes to the $l = 1$ term inside the star, but they are one order of magnitude smaller than this dipolar term outside the star.

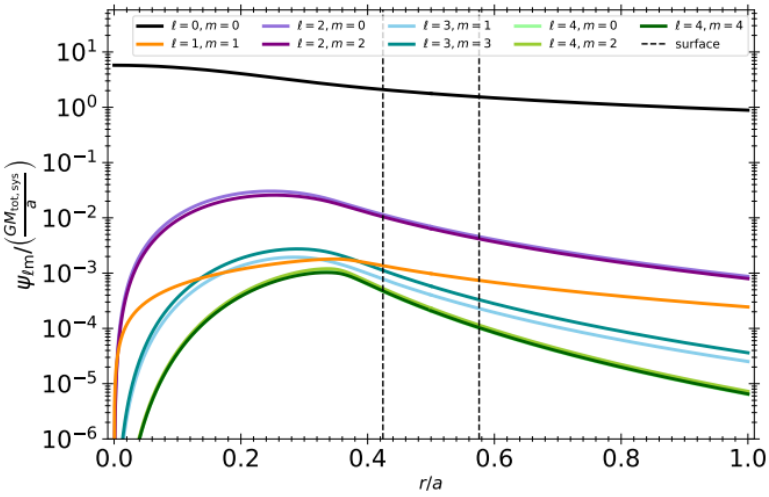

Figure 3.2: Normalized gravitational potential projected on the spherical harmonics of a star of $0.2M_\odot$ in a twin binary system with an orbital separation of $a = 2.8R_{1D}$. The dotted lines are corresponding to the surface of each star of the system in the direction including the most distorted point of each star and the Lagrangian point L1 ($\mu = 0, \phi = 0$). This Figure is directly taken from the article by L. Fellay [5] (Fig.9 p.12).

In Figure 3.3 is presented the Clairaut-Radau parameter, for $l = 2$, as defined by Equation 2.51. Its value is assumed to be the leading contribution by the perturbation model to the apsidal motion of binary systems. When comparing the Roche model to other models, both perturbative and MoBiDICT models predict significant differences in η_2 for all stars. These differences indicate the limitations of the Roche model in accurately representing stellar deformations due to assumptions about the stellar gravitational potential. In the less distorted regions of the star (when $r < 0.5R_{1D}$), similar results are obtained with both models, suggesting that the new modelling provides a good representation of stellar deformation in these regions, where the perturbative modelling is expected to be valid. However, as $r > 0.5R_{1D}$ (i.e., in the upper layers of the star), significant differences between the two models emerge, with discrepancies increasing with r, as the stellar deformations become more pronounced. These differences can be attributed to the limitations of the perturbative approach in regions of high deformation, whereas this new non-perturbative model is specifically designed to study such cases.

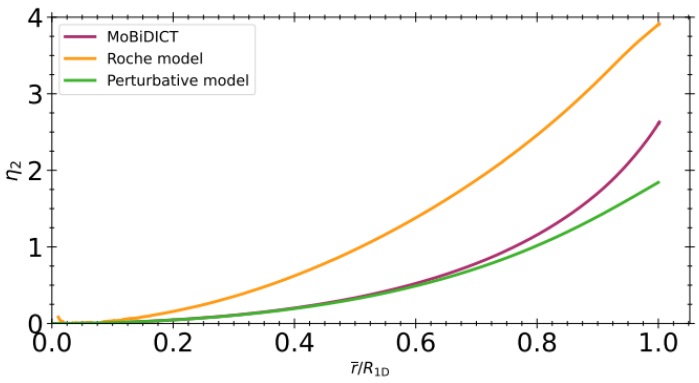

Figure 3.3: Evolution of η_2 as a function of the average radius for the different models studied in this work. The system studied here is a twin binary system composed of two $0.2M_{\odot}$ stars with an orbital distance of $2.8R_{1D}$. This Figure is directly taken from the article by L. Fellay [5] (Fig.10 p.12).

3.3 Perspectives

Numerical noise arising from higher spherical orders of the potential and densities has been observed, which affects the accuracy of the derived η_l coefficients. To address this issue, it is planned to implement a coupling of MoBiDICT with a refined perturbative approach in the least distorted regions of the binary system. This refined approach will consider all the spherical orders and include terms of the tidal and centrifugal potential that are typically neglected in the classical perturbative models.

Moreover, several assumptions have been made for the computation of this code. The rotation axis of both stars is aligned with the orbital rotation axis, and we work in a synchronous configuration. A future plan is then to implement MoBiDICT such that it can support non-synchronized systems, as well as the misalignment of the axes of rotation of the systems. It has to be mentioned that this latest goal will destroy the symmetry inside the system.

4 Results

In this section will be presented the results obtained through the simulations using MoBiDICT, for a specific system that will be described. They will be compared first to the results obtained with the perturbative method, and then to the results computed from observations. Finally, the influence of the alpha overshooting on the apsidal motion will be shown.

4.1 System studied

In order to assess the results obtained through MoBiDICT simulations, it has been decided to study a system already observed experimentally by S. Rosu & al. [6]. This system, called HD152248, is a massive eccentric binary located in the core of the open cluster NGC 6231. It contains two twin stars, in a close binary configuration, which makes this system ideal to be simulated by MoBiDICT. Different parameters, determined by both spectroscopic and photometric observations, are given in Table 4.1.

Absolute masses	$29.5^{+0.5}_{-0.4} M_\odot$
Orbital period	$5.816498^{+1.6e-6}_{-1.8e-6}$ d
Eccentricity	0.130 ± 0.002
Inclination	$67.6^{+0.2\circ}_{-0.1}$
Effective temperature	34000 ± 1000 K
Bolometric luminosities	$(2.73 \pm 0.32) \times 10^5 L_\odot$
Mean stellar radii	$15.07^{+0.08}_{-0.12} R_\odot$
Apsidal motion rate	$1.843^{+0.064\circ}_{-0.083}$/yr

Table 4.1: Parameters of the twin stars inside the binary system HD152248, obtained through spectroscopic and photometric observations. Those parameters come from Rosu& al. article [6].

From those parameters, Rosu & al. aimed to construct stellar evolution models using the Clés code, and incorporate various prescriptions for internal mixing within the stars. They try to identify models that best fit the observationally determined properties of the components of HD 152248, including their internal structure constants and apsidal motion rate. Several models are already presented in their article, but this chapter will aim to examine the impact of the more accurate calculation made by the non-perturbative method on the determination of some parameters, comparatively to the perturbative method.

To compute the initial properties of the system that will be used in MoBiDICT, we choose to study a system with mass loss. The input parameters are presented in Table 4.2. They result from the latest model presented by Rosu & al. [6] in their Table 1, page 7. Moreover, mixing in convective regions is parameterized using the mixing length theory, where the parameter $\alpha_{\rm ov}$ will be defined. It is the overshooting parameter chosen by the user that will displace the boundary of the mixed region inside the star structure, such that:

$$r_{ov} = r_c + \alpha_{ov} \min(H_p(r_c), h), \tag{4.1}$$

with r_c the Ledoux limits' radius of the convective zone, r_{ov} the new boundary radius, h is the thickness of the convective layer, and $H_p(r_c) = P(r_c)/\rho(r_c)\ g(r_c)$ represents the pressure scale height taken at the edge of the convective core as determined by Ledoux criterion. A study of the influence of α_{ov} on several parameters inside the system will be done in the last section, but for the first comparisons, we will consider $\alpha_{ov} = 0.4$. In addition to convective mixing, turbulent diffusion is considered inside the star.

Initial mass	32.8 ($M_\odot$)
Mass loss rate	$1.17e-6 (M_\odot/\mathrm{yr})$
Metallicity	0.015
Hydrogen mass fraction	0.715
Turbulent diffusion coefficient	$-1.6e7$

Table 4.2: Input parameters to the CLÉS code for the computation of the stellar evolution models.

Once the stellar evolution of the star is computed, the exact model we will use is determined via the value of the mean radius. We choose the step for which the radius of the star is the closest possible to $15.07 R_\odot$, and take the structure of the star at this specific step. We have then the initial model for the density profile that we will enter as initial conditions to MoBiDICT.

4.2 Comparison between MoBiDICT and perturbative method

It has been shown by L. Fellay that both MoBiDICT and perturbative methods give the same results in the less distorted regions. Another way to assess this conclusion is to study the potential obtained via both methods with respect to the distance between both stars. Indeed, if the stars are further away, the distortion of their shape will be less important. This can be seen in Figure 4.1 and 4.2, where the gravitational potential evaluated at the surface is shown for the dominating terms $\Phi_{2,0}$ and $\Phi_{2,2}$, depending on the distance between both stars, normalized with respect to the radius of the star. For large distances, both potentials seem to be the same. On the contrary, for closer systems, we directly see a difference between them. The minimal distance considered here is $a = 2R_1$ as, under this distance, MoBiDICT is not able to compute a numerical solution, essentially because the two stars are in contact.

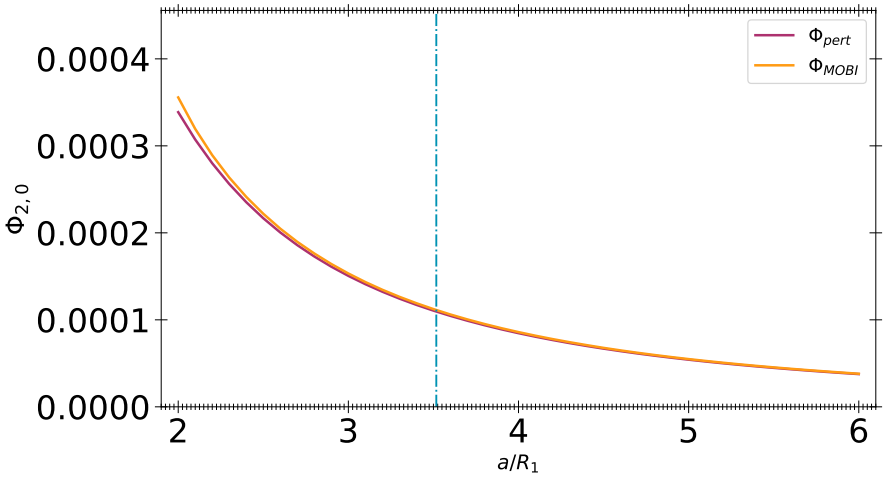

Figure 4.1: $\Phi_{2,0}$ with respect to $a/R1$. a is the distance between both stars' centers, and $R1$, the radius of the star. The blue dash line corresponds to the distance in the system HD152248 studied.

The difference between dominant potentials is illustrated in Figure 4.3, where is shown the relative difference between the MoBiDICT potential and the perturbative potential. This figure allows us to notice that even for high distances systems, there is a variance of 1 and 2%, respectively for $\Phi_{2,0}$ and $\Phi_{2,2}$. This difference is all the greater as the distance between the stars decreases, reaching respectively 5 and 17%. In the HD152248 system, the distance between both stars is 3.5169 R_1, and the corresponding error between both methods is equal to 1.5% for $\Phi_{2,0}$ and 3.6% for $\Phi_{2,2}$.

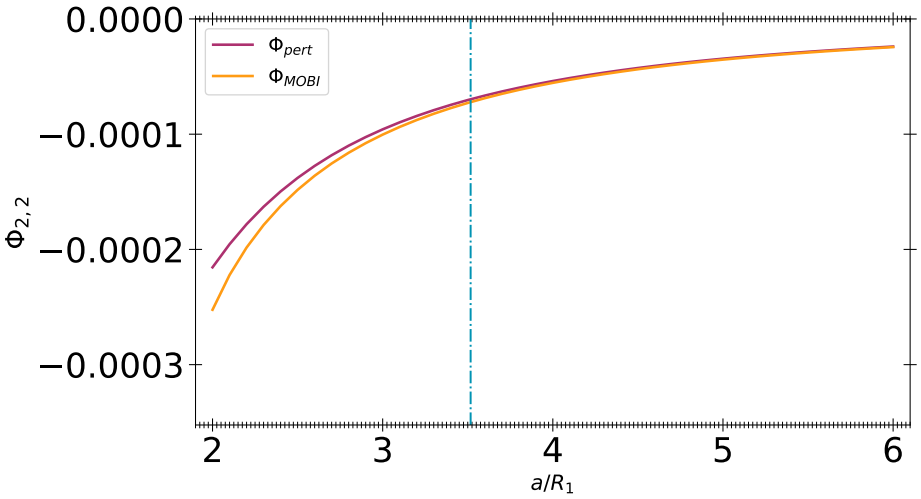

Figure 4.2: $\Phi_{2,2}$ with respect to $a/R1$. a is the distance between both stars' centers, and $R1$, the radius of the star. The blue dash line corresponds to the distance in the system HD152248 studied.

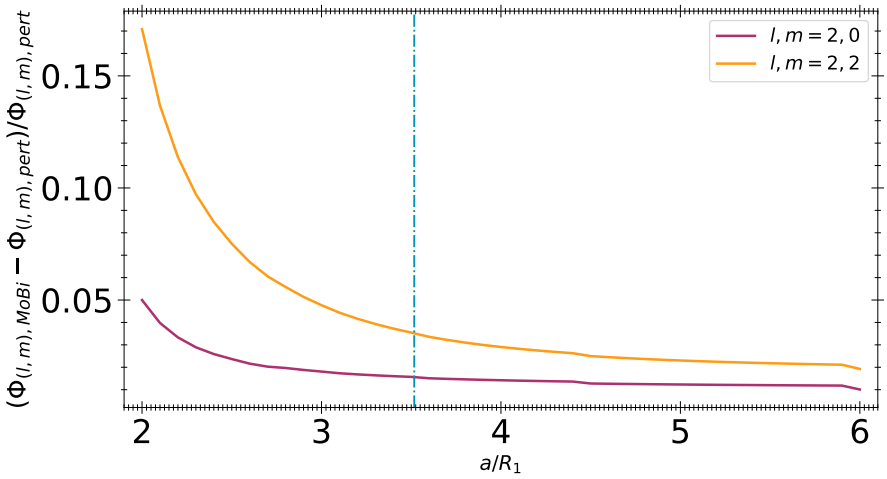

Figure 4.3: Relative difference between the potential computed by MoBiDICT and via the perturbative method, for the dominant spherical terms, with respect to $a/R1$. a is the distance between both stars' centers, and $R1$, the radius of the star. The blue dash line corresponds to the distance in the system HD152248 studied.

A last spherical term of the potential to study is the dipolar term, for $l = 1$. The perturbative method assumes that it is negligible. However, when looking at Figure 4.4, one can see the ratio between the dipolar term and the term for $l, m = 2$, as a function of the distance between the stars. For high distances, this dipolar term is negligible. However, for close systems, it has to be taken into account, as this ratio tends to be 10%.

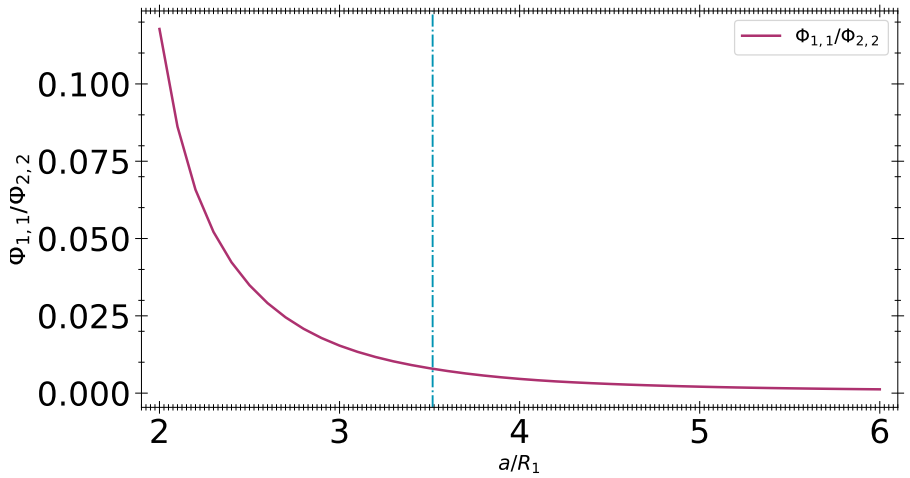

Figure 4.4: $\Phi_{1,1}/\Phi_{2,2}$ with respect to $a/R1$. a is the distance between both stars' centers, and $R1$, the radius of the star. The blue dash line corresponds to the distance in the system HD152248 studied.

Those results conclude with the same deductions as obtained by L. Fellay. For wide binary systems, the perturbation method is enough to model the distortion of the stars. However, for close binaries, the dipolar term takes more importance such that it can be neglected anymore, as it is usually done in the perturbative method. To determine which method is best able to represent the deformations in the system, a comparison with observational data will be done in the next section.

4.3 Comparison with observational data

The value of the apsidal motion rate has already been computed for the system HD152248, as written in Table 4.1. The value $\mathscr{R}$ can be computed from the potentials obtained via MoBiDICT or the perturbation method. This $\mathscr{R}$ is the perturbation that will provoke the apsidal motion inside the system, as presented for the perturbation method in Equation 2.96. However, in MoBiDICT, the value of $\mathscr{R}$ will be normalized by GM/a. In Figure 4.5 are shown those values. Once again, for close binaries, the perturbative method will give an inferior result to the one computed by MoBiDICT.

It is also possible to compute the value of the apsidal motion rate via Equation 3.12 using MoBiDICT. This value is equal to $\dot{\omega}_{MoBi} = 1.80°/\text{yr}$. However, the value computed from observational data contains a relativistic term that must be taken into account. This relativistic term can be expressed as:

$$\dot{\omega}_{GR} = \left(\frac{2\pi}{P_{\text{orb}}}\right)^{5/3} \frac{3\,[G(M_1+M_2)]^{2/3}}{c^2(1-e^2)}. \tag{4.2}$$

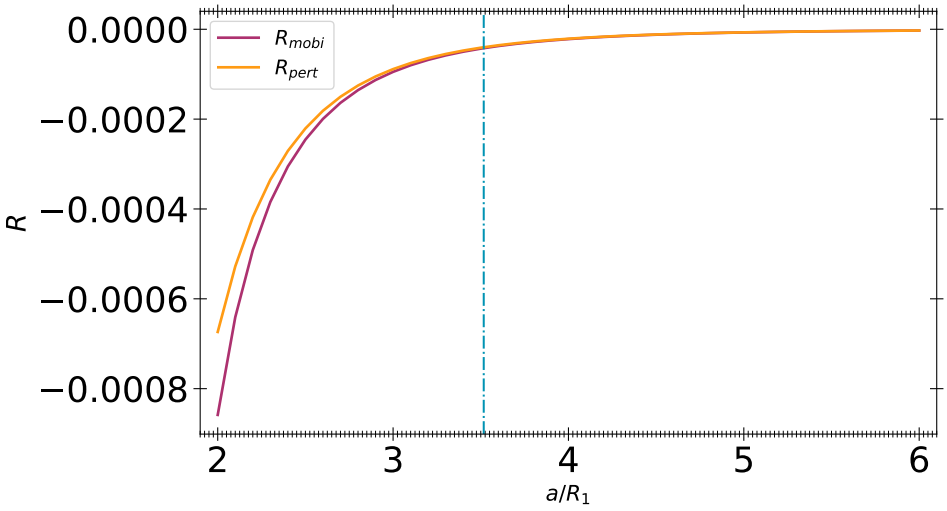

Figure 4.5: $\mathscr{R}$ as a function of $a/R1$. $\mathscr{R}$ is the perturbation that will induce the apsidal motion, a is the distance between both stars' centers, and $R1$, the radius of the star. The blue dash line corresponds to the distance in the system HD152248 studied.

Replacing inside this equation the value from Table 4.1, and considering the value $M_1 = M_2 = 29.5 M_\odot$, we obtain for the relativistic component the value:

$$\dot{\omega}_{GR} = 0.163°/\text{yr}. \tag{4.3}$$

If we subtract this contribution from the total apsidal motion rate observed, given in Table 4.1, we have $\dot{\omega} = 1.68°/\text{yr}$, for the observational data. It is only 7.1% difference from the results obtained with MoBiDICT. This new non-perturbative method will then overestimate the value of the apsidal motion rate, even if this difference is not that high. In the next section will be shown how the apsidal motion will be impacted by the parameter α_{ov}.

4.4 Influence of the alpha overshooting

We search here how the α_{ov} will influence the results obtained via the simulations, as the internal structure of the stars will be different. These differences in internal structures will be reflected through the apsidal motion rate, but also via the parameter k_2 and the estimated age of the system.

As said, the first and most important parameter to look at is the apsidal motion rate. In Figure 4.6 is presented the apsidal motion rate obtained from the perturbation method, from MoBiDICT, but also the value from the observation of the system HD152248, as a function of the alpha overshooting. It is clearly seen that the perturbation method underestimates the value of the apsidal motion rate. This will induce also an underestimation of the internal characteristics of the stars. As the parameter α_{ov} increases, the apsidal motion rate will

decrease. A possible explanation for this phenomenon could be that the increasing of α_{ov} could decrease the efficiency of tidal interactions, as α_{ov} will affect the outer layer of the star. This reduced tidal interaction may lead to a slower apsidal motion rate.

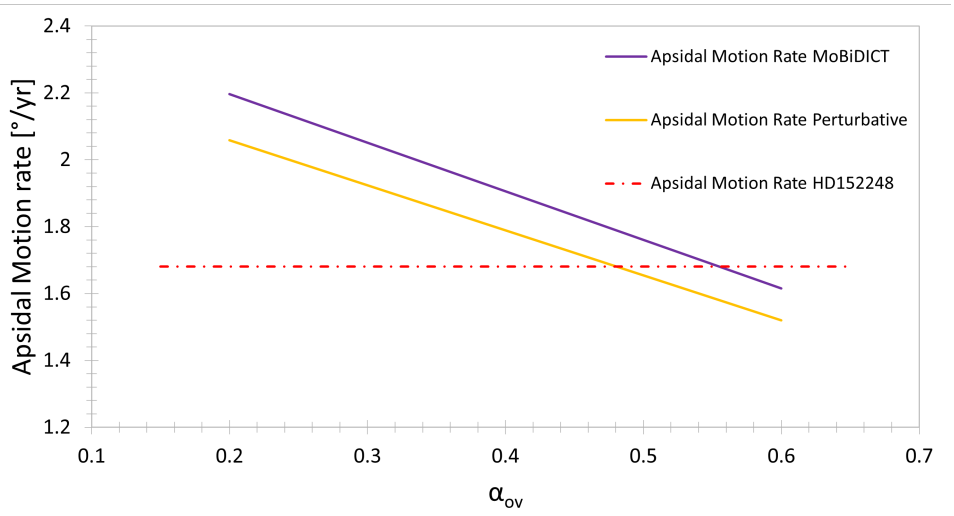

Figure 4.6: Evolution of the apsidal motion rate with respect to α_{ov}.

To analyze the influence of α_{ov}, we also compute the value of k_2 and of the Age of the system for values between 0.2 and 0.6. Those estimations are presented in Figure 4.7 and 4.8. It can be seen that an increase of α_{ov}, i.e. a displacement of the boundary of the convection region, will decrease the value of k_2. This number is related to the distribution of mass within the star and provides then insights into its internal density and the deformations caused by tidal forces. A decrease in k_2 indicates that the star's internal structure is less affected by tidal forces. This might be the result of a more compact and centrally concentrated mass distribution. A more massive and denser core compared to the outer layers could lead to a decrease in k_2, as the central region dominates the overall tidal response.

On the other end, the estimated age will also provide details concerning the internal structure of the stars. By comparing the observed value of k_2 to theoretical models of tidal evolution, astronomers can estimate the age of the binary star system. The process involves backward modelling to determine how much time would have been required for the system to evolve from a more eccentric state to its current state with the observed k_2 value. In Figure 4.8, we can see that this estimated age will increase as we increase the boundary of the convection zone. Different internal structures lead to different tidal evolution rates and, consequently, different age estimates. Systems with more centrally condensed masses or lower deformability may have longer tidal circularization timescales, resulting in older age estimates.

The α_{ov} directly influences the internal structure of the stars inside the binary system. It

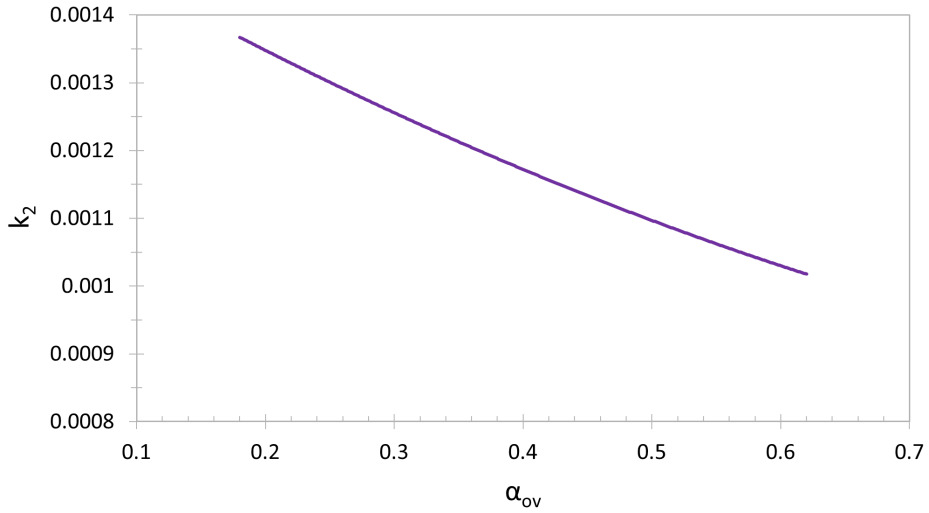

Figure 4.7: Evolution of the apsidal motion's constant with respect to α_{ov}.

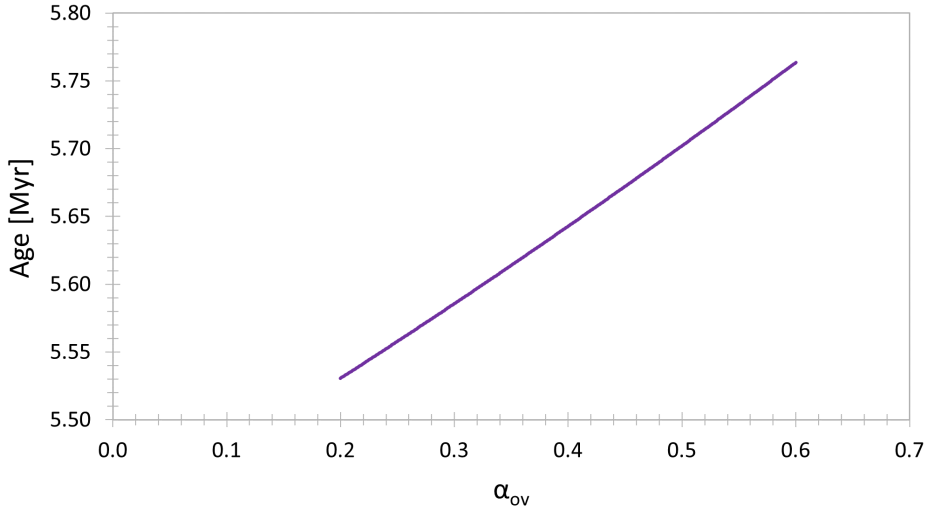

Figure 4.8: Evolution of the estimated age of the system with respect to α_{ov}.

is observed through, in particular, the apsidal motion's constant and the estimated age of the system. By observing a system, as it has been done for HD152248, it is possible to estimate the internal structure of the stars, and then have a better comprehension of the phenomenon appearing inside this kind of system.

5 Conclusion

In binary star systems with close proximity, the interplay of tidal interactions and rotational effects plays a crucial role in influencing stellar evolution. This work embarks on a two-fold mission. Initially, it involves a comprehensive expansion of the perturbative model to highlight simplifications and gauge their impact as potential errors on binary systems' parameters. Subsequently, a comparison is drawn between this perturbative model and MoBiDICT [5], an innovative non-perturbative 3D static model designed to calculate deformations in binary systems. Furthermore, these findings are juxtaposed with those of a previously studied system by S. Rosu [6] to validate their relevance.

In the first section of this work is presented a general definition of a binary star system. The different types of classification for those systems are discussed. The first one is based on the separation distance between both stars. The second one refers to the interaction between them, depending on the filling of their respective Roche lobe. Finally, the third classification is based on their method of detection. The formation of this kind of system is then explored, as the exact conditions of formation are still investigated. Subsequently, the evolution of binaries is discussed, as it depends on several interactions between both stars, i.e. mass transfer, tidal effects, common envelope evolution and even stellar merger. The case of multiple-star systems is then considered. Finally, the possible presence of planets in binary systems is reviewed. The objectives and outlines of the current work are then given, and finally, a quick literature review is presented on the theoretical and numerical works already done.

Thereafter, the second section is dedicated to theoretical advancements within the perturbative method. Using spherical harmonics, the derivation of apsidal motion within the binary star system is undertaken. This entails the development of the Clairaut-Radau equation, along with the expansion of various potentials including mutual gravitational potentials and the centrifugal potential. Afterwards, the expression for apsidal motion is derived based on the preceding outcomes. Several simplifications are highlighted by those develop-

ments. We consider the rotation of the stars as a solid body rotation, such that the centrifugal force derives from a potential. We also assume a small eccentricity, so that the spheroids, shaping both stars, are nearly spherical. The second star is treated as a punctual source by the first one. Finally, several expressions are approximated at first order.

In the third section is presented MoBiDICT, a new non-perturbative method used to compute the structural deformations in close binary systems in three dimensions. A general description of the code's working is given, as well as the computation of the apsidal motion rate. A first comparison with Roche and perturbative models has been done by L. Fellay and is resumed. It is shown that for close binaries, Roche model does not predict the deformation as well as MoBiDICT does. Concerning the perturbative model, it appears to be close to MoBiDICT's results when the stars are not highly deformed. Finally, the perspectives of MoBiDICT are discussed, notably a possible coupling with the perturbative model in the least distorted regions in order to save some numerical noise.

Finally, the last section is dedicated to the results obtained through the simulations using MoBiDICT. The first part introduces an existing system that has been observed by S. Rosu [6], HD152248. This system is a twin binary system, and the parameters characterising both stars and the orbit are given.

The second part is a comparison between MoBiDICT and the perturbative method. The dominant spherical terms, $\Phi_{2,0}$ and $\Phi_{2,2}$ are computed for different value of a, the distance between stars' centers. We can see that for closer systems, the relative difference between the perturbative and MoBiDICT calculations is higher than for further systems. In the closest cases, we can reach a difference of 5% and 17% for respectively $\Phi_{2,0}$ and $\Phi_{2,2}$. In the case of HD152248, for which the separation distance is equal to $3.5169R_1$, those errors are respectively equal to 1.5% and 3.5%. Finally, the influence of the dipolar term is studied. In the perturbative method, this term is assumed as negligible. However, we showed that for close binaries, i.e. for high distortions, it cannot be neglected as it is equivalent to 10% of the $\Phi_{2,2}$ term.

The third part is a comparison between the simulations by MoBiDICT of the system HD152248 and its observational data. With MoBiDICT, we obtain an apsidal motion rate equal to 1.80°/yr, which has a difference of only 7.1% with the observational data.

Finally, the fourth part shows the influence of the parameter alpha overshooting. First, we present the apsidal motion rate computing with the perturbative method and with MoBiDICT. On one side, we see that the perturbation method underestimates the value of this apsidal motion rate, and we conclude that this is due to the approximation made by the perturbation method. On the other side, we see that the apsidal motion decreases as α_{ov} increases. We explain this by the fact that α_{ov} modifies the outer layer of the stars, so that it will decrease the efficiency of tidal effects. The apsidal motion's constant k_2 as well as the

estimated age have also been studied depending on the value of α_{ov}. k_2 is also inversely proportional to alpha overshooting. As this number directly relies on the internal density of the stars, we conclude that an increase in the convective region zone will lead to reduced tidal interactions. Finally, the estimated age has also been investigated, and as α_{ov} increases, the age will also increase. Systems exhibiting greater central mass concentration or reduced deformability might experience extended tidal circularization timescales, leading to the derivation of older age estimations.

Bibliography

[1] J.E. Pringle, On the formation of binary stars, *Mon. Not. R. astr. Soc.* (1989) 239, 361-370.

[2] S. Offner, M. Dunham, K. Lee, H. Arce, D. Fielding, The turbulent origin of outflow and spin misalignment in multiple star systems, *The Astrophysical Journal Letters*, 827:L11 (6pp), 2016 August 10. doi:10.3847/2041-8205/827/1/L11

[3] S. Offner, K. Kratter, C. Matzner, M. Krumholz, R. Klein, The formation of low-mass binary star systems via turbulent fragmentation, *The Astrophysical Journal*, 725:1485–1494, 2010 December 20. doi:10.1088/0004-637X/725/2/1485

[4] K. Kratter, G. Lodato, Gravitational Instabilities in Circumstellar Disks, *Annual Review of Astronomy and Astrophysics*, vol. 54, p.271-311. doi:10.1146/annurev-astro-081915-023307

[5] L. Fellay, M.-A. Dupret, MoBiDICT: new 3D static models of close, synchronized binaries in hydrostatic equilibrium, *Astronomy & Astrophysics manuscript*, May 24, 2023.

[6] Rosu, S., Noels, A., Dupret, M. A., et al., Apsidal motion in the massive binary HD152248, *A&A*, 642, A221, 2020.

[7] Rosu, S., Rauw, G., Nazé, Y., Gosset, E., & Sterken, C., Apsidal motion in massive eccentric binaries: The case of CPD-41° 7742, and HD 152218 revisited, *A&A*, 664, A98, 2022b.

[8] Kopal, Z. 1959, Close binary systems

[9] Kopal, Z. 1978, Dynamics of close binary systems

[10] J.L. Tassoul, Theory of rotating stars (PSA-1), *Princeton University Press*, Princeton, New Jersey, 1978.

[11] Shibahashi, H. (1991). The Effect of the Rotation of the Stellar Envelope on the Apsidal Motion in Close Binary Systems. *Publications of the Astronomical Society of Japan*, 43, 471-482.

[12] Claret, A., & Giménez, A. (1990). A Practical Method for the Computation of the Apsidal Motion. *The Astrophysical Journal*, 359, 313-318.

[13] Claret, A., & Giménez, A. (1993). The Apsidal Motion Test of the Internal Stellar Structure - Comparison Between Theory and Observations. *Astronomy and Astrophysics*, Vol. 277, NO. 2/OCT(I), P. 487, 1993

[14] A. Prs˘a and T. Zwitter, A computational guide to physics of eclipsing binaries, *The Astrophysical Journal*, 628:426–438, 2005.

[15] Wilson, R., Devinney, E., Van Hamme, W. WD: Wilson-Devinney binary star modeling, *Astrophysics Source Code Library*, record ascl:2004.004, 2020

[16] L. Siess, R. G. Izzard, P. J. Davis, and R. Deschamps, BINSTAR: a new binary stellar evolution code, *A&A* 550, A100 (2013)

[17] Fitzpatrick, R. 2012, An Introduction to Celestial Mechanics.

[18] R. Scuflaire, S. Theado, J. Montalban, A. Miglio, P.-O. Bourge, M. Godart, A. Thoul and A. Noels, CLES, Code Liégeois d'Évolution Stellaire, *Astrophysics and Space Science*, Vol. 316, pp.83-91, https://doi.org/10.1007%2Fs10509-007-9650-1